Cell Reports
Medicine

Article

Exercise intensity modulates interorgan communication and is associated with cardiometabolic health outcomes in humans

Graphical abstract

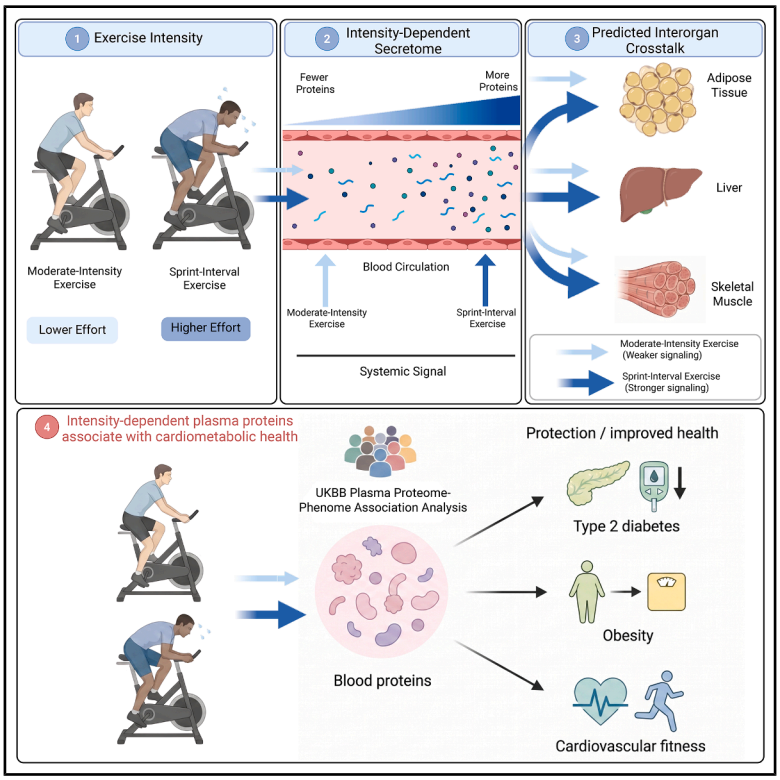

Highlights

- Exercise intensity shapes predicted interorgan communication
- SIE elicits greater circulating protein and metabolite responses than MIE
- SIE-stimulated proteins are preferentially associated with cardiometabolic protection

Authors

Luke Olsen, Javier Botella, Douglas Barrows, ..., Robert E. Gerszten, David J. Bishop, Paul Cohen

Correspondence

pcohen@rockefeller.edu

In brief

Sprint-interval exercise (SIE) is a time-efficient exercise prescription. However, how short bursts of physical activity promote metabolic health remains unclear. Olsen et al. show that SIE stimulates greater remodeling of plasma, skeletal muscle, and adipose tissue than moderate-intensity exercise, suggesting that predicted interorgan crosstalk may contribute to SIE's metabolic benefits.

Olsen et al., 2026, Cell Reports Medicine 7, 102988
September 15, 2026
https://doi.org/10.1016/j.xcrm.2026.102988

CellPress

Cell Reports Medicine

CellPress
OPEN ACCESS

Article

Exercise intensity modulates interorgan communication and is associated with cardiometabolic health outcomes in humans

Luke Olsen,[1] Javier Botella,[2,3] Douglas Barrows,[4] Ethan Romero,[5] Kaitlyn Baird,[6] Mutsumi Katayama,[7] Ece Kilic,[8] Christopher Peralta,[8] Nadège Zanou,[3] Henry Sanford,[9] Laurie Farrell,[10] Christopher L. Axelrod,[11] Kaja Plucińska,[1] Jeanne Walker,[12] Lu Yan,[13] Katie Fredrickson,[10] Olivier Pourquie,[13] Jeremy M. Robbins,[10] Ekaterina V. Vinogradova,[9] Henrik Molina,[8] Nicolas Place,[3] John P. Kirwan,[11] Juleen R. Zierath,[14] Anna Krook,[7] Robert E. Gerszten,[10] David J. Bishop,[2] and Paul Cohen[1,15,*]

[1]Laboratory of Molecular Metabolism, The Rockefeller University, New York, NY 10065, USA
[2]Institute for Health and Sport, Victoria University, Melbourne, VIC, Australia
[3]Institute of Sport Sciences and Department of Biomedical Sciences, University of Lausanne, Lausanne, Switzerland
[4]Bioinformatics Resource Center, The Rockefeller University, New York, NY 10065, USA
[5]Weill Cornell Medical College, New York, NY 10065, USA
[6]Department of Rehabilitation and Performance, Hospital for Special Surgery, New York, NY 10021, USA
[7]Department of Physiology and Pharmacology, Karolinska Institutet, 171 76 Stockholm, Sweden
[8]Proteomics Resource Center, The Rockefeller University, New York, NY 10065, USA
[9]Laboratory of Chemical Immunology and Proteomics, The Rockefeller University, New York, NY 10065, USA
[10]Division of Cardiovascular Medicine, Beth Israel Deaconess Medical Center, Boston, MA 02215, USA
[11]Integrated Physiology and Molecular Medicine Laboratory, Pennington Biomedical Research Center, Baton Rouge, LA 70808, USA
[12]The Rockefeller University Hospital, New York, NY 10065, USA
[13]Department of Genetics, Harvard Medical School, Boston, MA 02115, USA
[14]Department of Molecular Medicine and Surgery, Karolinska Institutet, 171 76 Stockholm, Sweden
[15]Lead contact
*Correspondence: pcohen@rockefeller.edu
https://doi.org/10.1016/j.xcrm.2026.102988

SUMMARY

Exercise is an integral therapy for many cardiometabolic diseases, including obesity, type 2 diabetes, and hypertension. Despite its broad health benefits, the circulating factors that mediate exercise adaptations in humans remain incompletely defined, particularly across different exercise intensities. Here, we conducted a multi-cohort human exercise intervention incorporating sprint-interval exercise (SIE) and moderate-intensity exercise (MIE) to analyze intensity-dependent regulation of interorgan crosstalk. We found that exercise intensity distinctly influenced the plasma proteome and metabolome in untrained and trained participants. By integrating multi-organ gene and protein expression datasets with *in vitro* and *in vivo* tissue sampling, we mapped regulated proteins to their predicted tissues of origin and destination. Muscle fibers and adipocytes were particularly sensitive to exercise intensity and observed to undergo broad secretory and transcriptomic changes. Moreover, we leveraged a large-scale plasma-phenome database to identify intensity-dependent proteins associated with cardiometabolic health and disease, highlighting how exercise intensity differentially shapes interorgan communication and organismal health.

INTRODUCTION

The metabolic benefits of regular exercise reflect a coordinated multi-organ response, spanning distant tissues and diverse cell types. Secreted metabolites, lipids, peptides, and proteins govern exercise-regulated interorgan crosstalk and contribute substantially to exercise-dependent adaptations.[1] In addition to upregulating secretory factors, termed exerkines,[2] exercise also downregulates the levels of deleterious factors. Collectively, these circulating mediators (the secretome) regulate multiple aspects of metabolism, such as promoting adipose tissue remodeling by reducing fibrosis while increasing vascularization and innervation,[3–5] enhancing whole-body glucose handling through metabolic rewiring in skeletal muscle,[6] and improving cognition through stimulating neurogenesis and inhibiting neuroinflammation.[7]

Increasing evidence suggests that not all exercise is equal. Distinct exercise intensities, such as sprint-interval exercise (SIE) or moderate-intensity exercise (MIE), elicit intensity-dependent, body-wide adaptations,[8] that may, in part, be driven by differences in secretory profiles.[9,10] Supporting this, *N*-lactoyl-phenylalanine (Lac-Phe), a recently described obesity-mitigating metabolite, is secreted following exercise in an

Please cite this article in press as: Olsen et al., Exercise intensity modulates interorgan communication and is associated with cardiometabolic health outcomes in humans, Cell Reports Medicine (2026), https://doi.org/10.1016/j.xcrm.2026.102988

intensity-dependent manner, with greater secretion following sprint exercise relative to resistance or endurance exercise.[11,12] Similarly, many soluble proteins, such as interleukin 6 (IL-6) and growth differentiation factor 15 (GDF15), are also secreted in an intensity-dependent manner, resulting in broad and context-dependent metabolic changes.[13–15] Characterizing intensity-dependent secretory responses may uncover how SIE—often lasting less than 5 min of total work—results in similar, if not superior, whole-body metabolic adaptations compared with longer-duration, low-intensity exercise or MIE.[16]

Despite the growing evidence suggesting intensity-dependent regulation of the plasma proteome and metabolome, in-depth comparisons following acute and chronic training interventions remain limited. Additionally, the identity of the tissue of origin and destination following different exercise intensities has been largely unexplored in humans. To address these key knowledge gaps, we characterized the plasma proteome and metabolome following a single session of SIE and MIE in participants before and after 8 weeks of training (hereafter termed untrained and trained). Incorporating a multiplexed, antibody-based protein detection platform, in combination with untargeted metabolomics, we uncover striking intensity-dependent changes to the plasma secretome in both untrained and trained participants and further characterize their predicted tissue of origin and target tissue. Notably, we identify multiple intensity-dependent circulatory factors linked with protection from cardiometabolic disease. Collectively, these findings provide insights into diverse intensity-dependent interorgan communication streams following exercise in humans and highlight potential causative factors contributing to the time-efficient health benefits attributed to high-intensity exercise.

RESULTS

The plasma proteome is differentially regulated by exercise intensity

To characterize acute changes to the plasma proteome following two distinct exercise intensities, we collected plasma before (rest), immediately following (0 h), and 3 h following (3 h) MIE (N = 9) or SIE (N = 10) in young, active, metabolically healthy males, as described previously.[17] MIE consisted of 90-min of continuous cycling at 90%–100% of the predetermined first lactate threshold, while SIE consisted of 6 sets of 30-s all-out cycling at a resistance of 0.075 $kg \cdot kg^{-1}$ body mass, with 4-min rests between the sets (Figure 1A). As anticipated and by design, blood lactate levels and pH were increased and decreased, respectively, immediately following SIE, with minimal change following MIE.[17]

To efficiently analyze the plasma proteome across its broad dynamic range, we used the antibody-based detection technology Olink Explore,[18] which detected and quantified 2,884 proteins across all participants and time points (Table S1). Critically, this pipeline reliably detected proteins, including IL-1β, IL-16, and IL-6, within the ng/mL–pg/mL range. Principal component analysis (PCA) revealed intensity-dependent changes to the plasma proteome, with samples collected immediately following SIE shifting along both PC1 and PC2 and returning to resting levels 3 h later (Figures S1A and S1C). In contrast, MIE showed no time-dependent clustering regardless of time point (Figures S1B and S1C).

SIE markedly altered the plasma proteome, with nearly a quarter (714 proteins) of the total detected proteins changing immediately following exercise (false discovery rate [FDR] < 0.05; Figures 1B and 1C; Table S1). Of these, >98%, including known exercise-responsive proteins growth hormone 1 (GH1), tissue inhibitor of metalloproteinase 3 (TIMP3), von Willebrand factor (VWF), and fatty acid-binding protein 5 (FABP5), showed increased abundance relative to resting levels. The number of differentially regulated proteins decreased by nearly 20-fold after 3 h, highlighting rapid changes to the plasma proteome following SIE. In stark contrast, only 7 proteins were differentially regulated immediately following MIE, and the number of such proteins increased to 19 after 3 h (Figure 1D; Table S1). MIE-regulated plasma proteins included follistatin (FST), insulin-like growth factor binding protein 1 (IGFBP1), and perilipin 1 (PLIN1). Despite minimal overlap between exercise intensities, both interventions increased GH1 and NAD-kinase (NADK) at 0 h, while decreasing prolactin (PRL), receptor activator of nuclear factor-β ligand (TNFSF11 [RANKL]), and fibroblast growth factor 19 (FGF19) after 3 h.

To more directly characterize intensity-dependent changes in the plasma proteome, we implemented a multifactorial analysis to test for an intensity × time interaction. This revealed 280 proteins at 0 h and 2 proteins at 3 h that were significantly different between SIE and MIE (FDR < 0.05; Table S1). Most differentially regulated proteins, including VWF, POMC, FABP5, and PLAT, showed increased abundance at 0 h following SIE relative to MIE, whereas the 2 differentially regulated proteins at 3 h, IGFBP1 and FST, were increased following MIE (Figure 1E). Importantly, many intensity-dependent changes remained significant after correction for exercise-induced shifts in plasma volume (see STAR Methods and Table S1) and were supported by an independent untargeted mass spectrometry (MS) analysis (see STAR Methods and Table S1). In fact, the MS-based analysis identified additional intensity-dependent proteins not present in the Olink assay, including the SIE-regulated proteins S100A6, CAPN1, and GSTO1 (Table S1).

To determine whether the observed changes to the plasma proteome are specific to the untrained state or persist in trained participants, we conducted an 8-week training regimen in a subset of the original participants, incorporating their respective mode of exercise: SIT (n = 7) or MIT (n = 6). Training consisted of 3–4 weekly sessions that gradually increased in intensity, duration, and frequency. After 8 weeks, the participants showed significant improvements in maximal aerobic power, 4-km time trial performance, and other cardiorespiratory fitness metrics across both training regimens.[17] Following 8 weeks of training, we conducted an identical acute exercise test and plasma processing pipeline, as described above. Intriguingly, plasma protein dynamics displayed similar temporal responses following acute exercise in the trained state, with an immediate increase following SIE, and a delayed increase following MIE (Figures S2A–S2C; Table S1), findings supported by significant correlations between the untrained and trained datasets (Figures S2D–S2G). Moreover, many of the shared and intensity-dependent changes persisted in the trained state, including

Please cite this article in press as: Olsen et al., Exercise intensity modulates interorgan communication and is associated with cardiometabolic health outcomes in humans, Cell Reports Medicine (2026), https://doi.org/10.1016/j.xcrm.2026.102988

CellPress
OPEN ACCESS

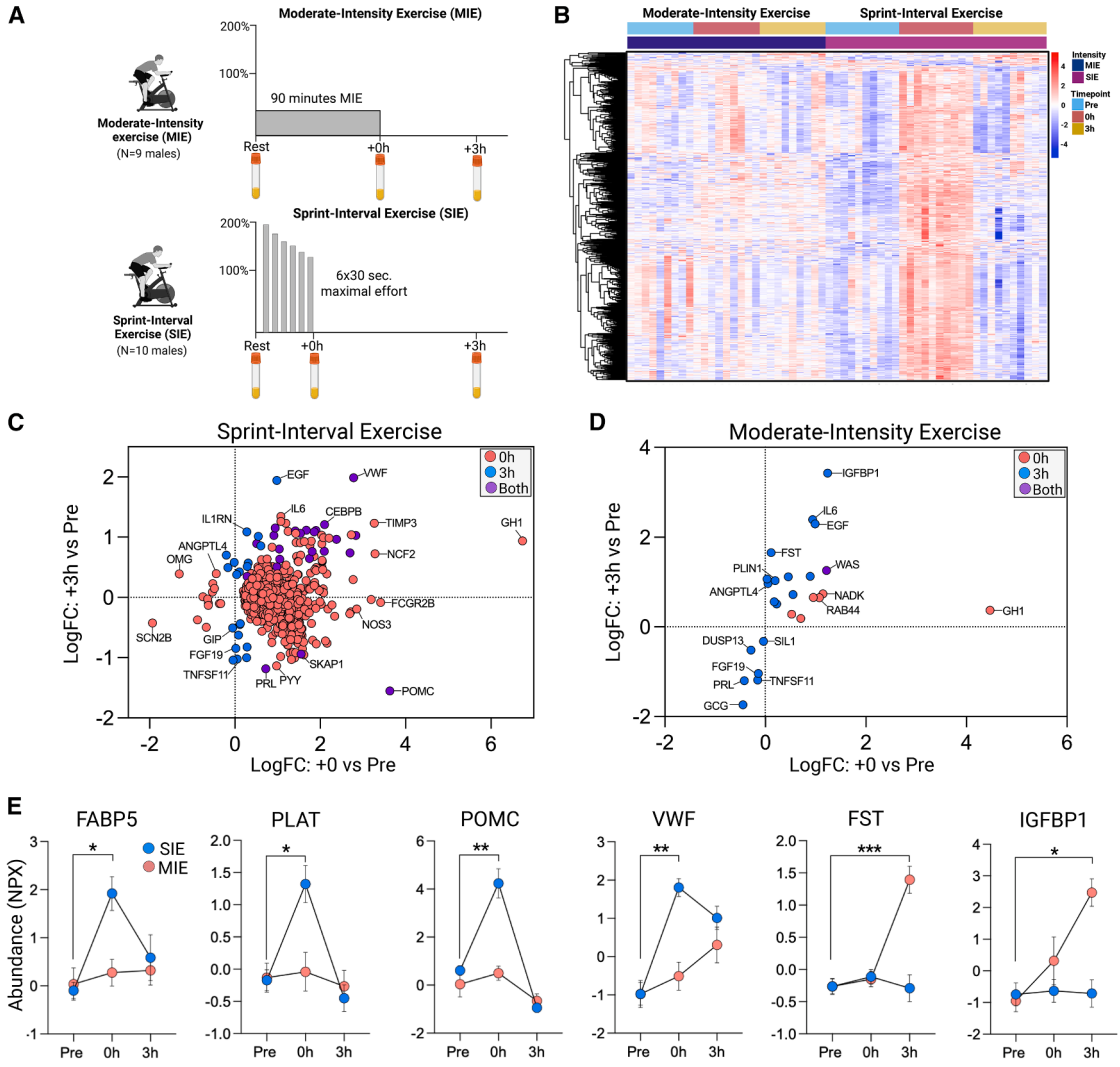

Figure 1. Acute SIE and MIE uniquely regulate the plasma proteome

(A) Experimental design for moderate-intensity exercise (MIE) and sprint-interval exercise (SIE). *N* = 9 and 10 male participants for MIE and SIE, respectively. (B–D) Heatmap showing *Z* scores of mean Olink NPX values for all differentially regulated proteins between pre and 0 h (immediately post) or 3 h (3 h post) following MIE or SIE. A scatterplot of the log fold change (logFC) for differentially regulated proteins between pre vs. 0 h and pre vs. 3 h for SIE (C) and MIE (D). (E) Plasma protein abundance of representative proteins in untrained participants following either SIE or MIE. Values are normalized protein values (NPX). Error bars indicate standard error of the mean. $^{*}p < 0.05$, $^{**}p < 0.01$, $^{***}p < 0.001$.

See also Figures S1 and S2.

GH1, VWF, and POMC (FDR < 0.05), as well as IGFBP1 and FST (nominal significance: $p < 0.05$) (Table S1). These data indicate that many acute changes in the plasma proteome are not unique to untrained individuals, but instead reflect the relative exercise intensity independent of training status.

Finally, we assessed the generalizability of our findings to commonly prescribed treadmill running, specifically to determine whether the low number of differentially regulated proteins following MIE is a result of the exercise intensity, modality (e.g., cycling), or a combination of the two. To test this, we collected and analyzed plasma samples from 9 healthy, active, trained male and female participants (*N* = 7 and 2, respectively) before and immediately following 2 h of running at 60% of their VO_{2max}[19]—an exercise regimen similar to MIE cycling. Using an identical protein processing pipeline as described above, we detected a total of 2,787 proteins, 111 of which were differentially regulated following exercise (Table S1). Of these proteins, nearly all (109 proteins) exhibited an increase relative to baseline (Figure S2H). Most of the shared proteins immediately following exercise were between SIE cycling and running, including ANGPTL4, VWF, FABP4, and ADAMTS1, suggesting that moderate-intensity running perturbs the plasma proteome to a greater extent than moderate-intensity cycling, at least, at the 0 h time point (Figures S2I and S2J). Nonetheless, the number of differentially regulated proteins following moderate-intensity running remained markedly lower than that following SIE, and

Please cite this article in press as: Olsen et al., Exercise intensity modulates interorgan communication and is associated with cardiometabolic health outcomes in humans, Cell Reports Medicine (2026), https://doi.org/10.1016/j.xcrm.2026.102988

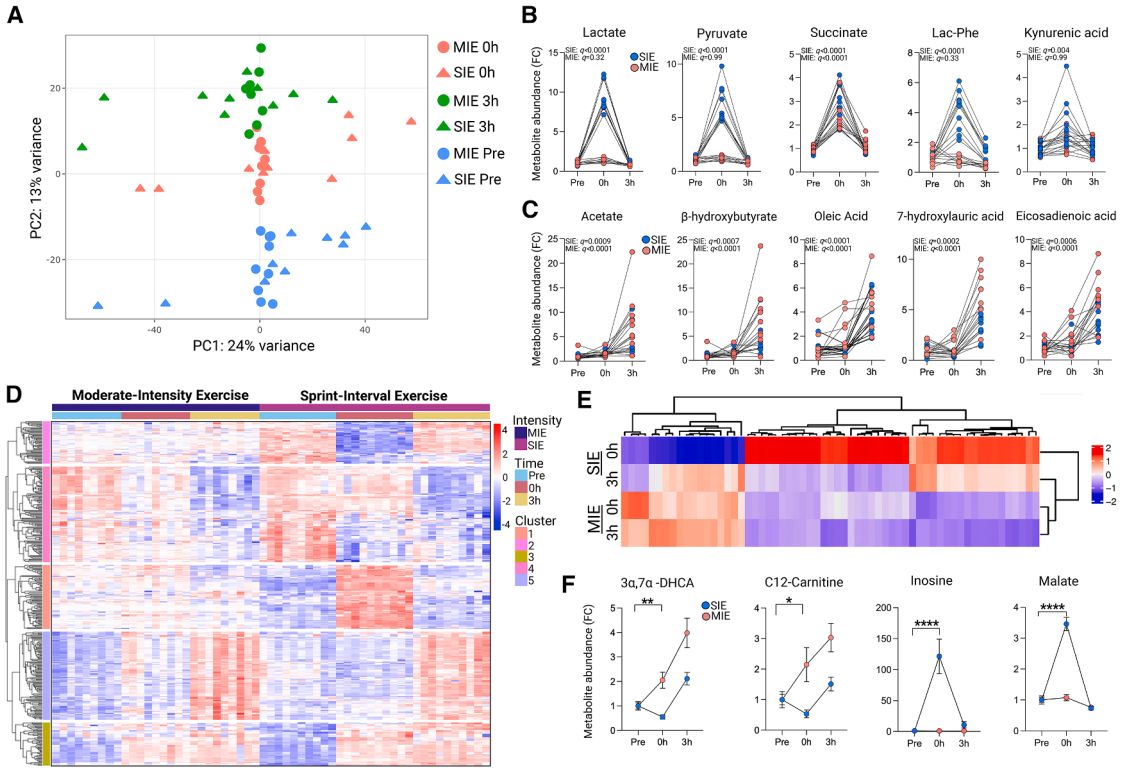

Figure 2. The plasma metabolome following SIE and MIE

(A–C) Principal component analysis of individual samples before ("pre"), immediately following ("0 h"), or 3 h following ("3 h") SIE or MIE. N = 9 and 10 male participants for MIE or SIE, respectively. Line plots showing representative metabolites and their corresponding q value, which peaks at 0 h (B) or 3 h (C).

(D) Heatmap showing all significantly changed metabolites and how they cluster by temporal expression patterns.

(E) Heatmap of the intensity-dependent significantly changed metabolites.

(F) Representative metabolites that were significantly changed between SIE and MIE. Error bars indicate standard error of the mean. $^{*}p < 0.05$, $^{**}p < 0.01$, $^{****}p < 0.0001$.

See also Figure S3.

this result highlights the dynamic circulatory changes following SIE compared with running or cycling at moderate intensities.

Intensity-dependent regulation of the plasma metabolome following SIE or MIE

While proteins have classically been studied for their endocrine function, secreted metabolites have become increasingly appreciated for their potential to act as molecular transducers, as highlighted by the characterization of exercise-responsive metabolites 2-hydroxybutyrate, Lac-Phe, β-aminoisobutyric acid, and 12,13-diHOME.[11,20–22] To identify additional metabolites secreted in an intensity-dependent manner, we performed untargeted polar plasma metabolomics following SIE or MIE and characterized the differential regulation of both annotated and unannotated metabolites (see STAR Methods).

In contrast to the plasma proteome (Figure S1C), the plasma metabolome exhibited intensity-dependent and time-dependent clustering following SIE and MIE, as revealed by the PCA (Figure 2A). SIE resulted in a total of 203 significantly changed metabolites immediately following exercise, including the well-described exercise-responsive metabolites lactate, succinate, malate, and pyruvate (Figure 2B; Table S2). We also found increases in lactate-derived metabolites after SIE, most notably Lac-Phe, which displayed similar temporal dynamics to circulating lactate (Figure 2B). Moreover, kynurenic acid—a metabolite secreted by skeletal muscle, which signals to adipose tissue[23]—increased following SIE, corresponding with a rise in circulating glycerol. At 3 h following SIE, 199 metabolites were significantly changed, including the fatty acids oleic acid, 7-hydroxylauric acid, and eicosadienoic acid. Strikingly, MIE again displayed a delayed response, with 31 significantly changed metabolites at 0 h, increasing to 183 metabolites at 3 h. Most of the changed metabolites were fatty acids, including acetate, beta-hydroxybutyrate, oleic acid, 7-hydroxylauric acid, and eicosadienoic acid (Figure 2C). Supporting these data, cluster-based analysis of all significantly changed metabolites revealed five distinct expression patterns, and most of them demonstrated time-dependent changes following SIE (Figure 2D; Table S2).

We next characterized significantly changed metabolites between exercise intensities through a multifactorial (time × intensity) analysis. We uncovered the greatest differences at the 0 h time point, with nearly all metabolites increasing following SIE relative to MIE (Figure 2E). These

Please cite this article in press as: Olsen et al., Exercise intensity modulates interorgan communication and is associated with cardiometabolic health outcomes in humans, Cell Reports Medicine (2026), https://doi.org/10.1016/j.xcrm.2026.102988

CellPress
OPEN ACCESS

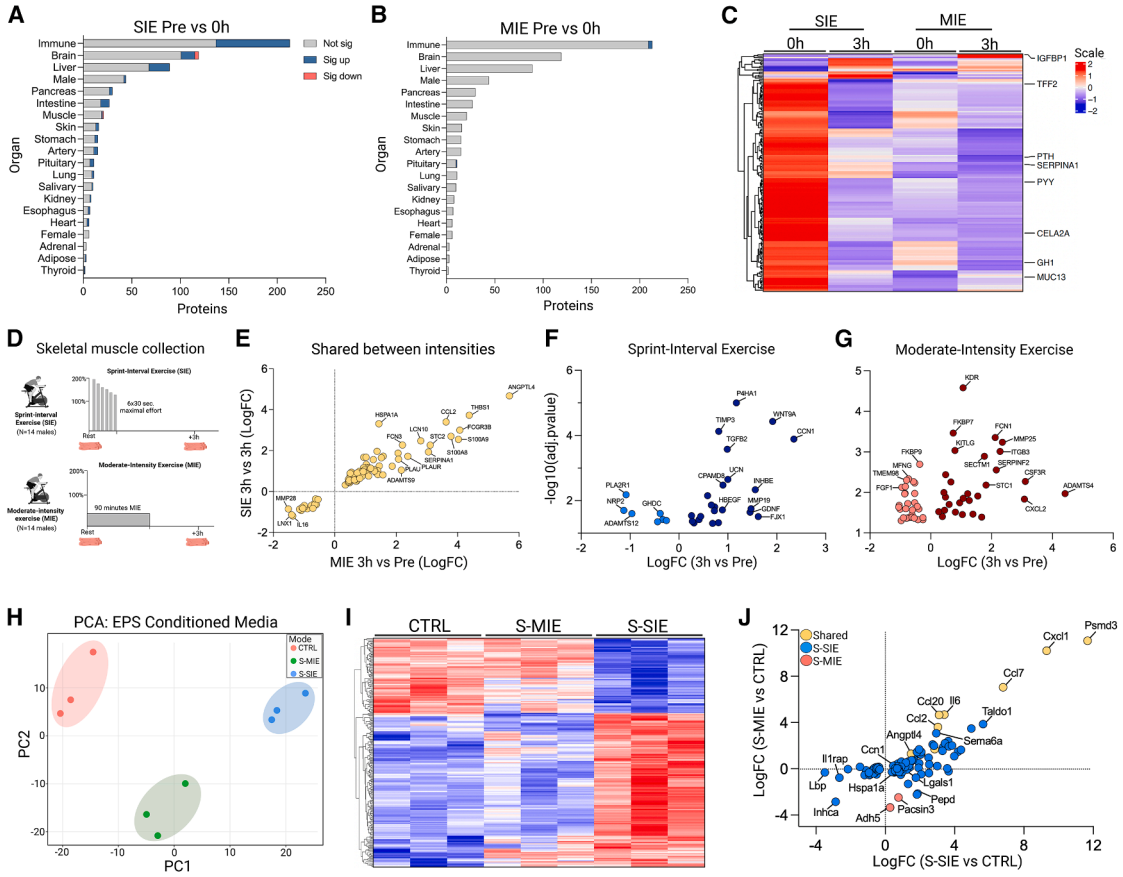

Figure 3. Identifying the tissue of origin for exercise-regulated plasma proteins

(A and B) All organ-enriched proteins with those increased (blue bar), decreased (red bar), or no change (gray bar) at 0 h following SIE (A) and MIE (B).

(C) A heatmap showing organ-enriched proteins differentially regulated at 0 h or 3 h following SIE and MIE.

(D–G) Schematic of the muscle collection time points following SIE and MIE. *N* = 14 male participants per condition. Predicted muscle-secretory genes differentially expressed following MIE and SIE (E), SIE-only (F), or MIE-only (G).

(H) Principal component analysis of the conditioned media proteome following no EPS (CTRL), simulated-MIE (S-MIE), and simulated-SIE (S-SIE).

(I) A heatmap of differentially regulated proteins detected in the conditioned media, with an FDR cutoff of 0.1.

(J) A scatterplot showing differentially regulated proteins between S-MIE versus CTRL and S-SIE versus CTRL.

The color scheme for (E)–(G) and (J) is as follows: yellow, shared; blue, SIE-specific; red, MIE-specific.

See also Figure S4.

included lactate, pyruvate, malate, and inosine, consistent with elevated glycolytic, tricarboxylic acid (TCA) cycle, and ATP turnover (Figure 2F). Despite relatively few changes immediately following MIE, increases in fatty acid-derived metabolites and bile acids, including C12-carnitine and 3α,7α-dihydroxycholanoic acid (3α,7α-DHCA), respectively, were observed immediately following MIE relative to SIE (Figure 2F). Notably, and in agreement with the results for the plasma proteome, many shared and intensity-dependent changes to the plasma metabolome persisted in the trained state, including those peaking at the 0 h (e.g., lactate, pyruvate, malate, inosine, and Lac-Phe) or 3 h time point (e.g., oleic acid, palmitic acid, linoleic acid, and eicosadienoic acid) (Figure S3; Table S2). Taken together, the results showed that the plasma metabolome displayed similar quantitative and temporal changes to the plasma proteome, further highlighting the unique intensity-dependent changes to blood-borne factors.

Multiple organs are predicted to contribute to the plasma proteome following exercise

We next sought to identify the predicted organ source(s) of exercise-responsive analytes, with a particular emphasis on proteins due to the challenging nature of identifying the cellular origin of circulating metabolites. To this end, we leveraged bulk human RNA sequencing datasets of diverse organs from the Genotype-Tissue Expression (GTEx) repository.[24] We considered a gene as enriched within a given organ if its expression in that organ was at least four times higher than its average expression in all other organs.[25] Using these criteria to filter differentially regulated plasma proteins following SIE, we found that immune-enriched proteins changed the most at both 0 h and 3 h, including AZU1, MNDA, and RAB44. Additional organ-enriched proteins following SIE were CELA2A (pancreas), PRL (pituitary), TFF2 (stomach), GUCA2A (intestine), CFHR5 (liver), PTH (thyroid), CNP (brain), EGLN1 (muscle), and FABP4 (adipose) (Figures 3A and 3C;

Please cite this article in press as: Olsen et al., Exercise intensity modulates interorgan communication and is associated with cardiometabolic health outcomes in humans, Cell Reports Medicine (2026), https://doi.org/10.1016/j.xcrm.2026.102988

Figure S4A; Table S3). Similar to SIE, immune-enriched proteins changed the most following MIE, again including AZU1 and RAB44. There was a greater distribution of organ-enriched proteins, including IGFBP1 (liver), PLIN1 (adipose), PRL (pituitary), GCG (pancreas), and DUSP13A (muscle) at 3 h following MIE (Figures 3B and 3C; Figure S4B; Table S3). Although the number of organ-enriched proteins decreased when filtering for those with a time × intensity interaction, several remained significant at 0 h following SIE, including the anti-inflammatory hormone ANXA1 (esophagus), the vasodilator CNP (brain), and POMC (pituitary). In contrast, only IGFBP1 (liver) remained enriched and differentially regulated at 3 h following MIE. Importantly, cross-referencing these organ-enriched genes with a multi-organ human proteomic dataset[26] strongly supported our gene-centric approach, thus further reinforcing their likely organs of origin.

To more directly identify tissue-derived proteins potentially missed using the above-described approach, we collected skeletal muscle from the *vastus lateralis* before and 3 h following SIE and MIE and performed bulk RNA sequencing (Figure 3D).[17] We chose skeletal muscle because of its documented intensity-dependent remodeling following exercise[27] and its role in interorgan crosstalk.[28] To identify transcripts predicted to encode secretory proteins, we overlaid the differentially expressed genes (DEGs) between SIE and MIE with a curated human secretome database from the Human Protein Atlas.[29] This approach revealed 111 and 140 DEGs following SIE and MIE, respectively, predicted to encode secretory proteins (Table S3). Of these, 81 genes were shared between exercise intensities, with 30 genes specific to SIE, and 59 genes specific to MIE. Many of the genes shared between exercise intensities encode well-described exerkines, including *ANGPTL4*, *VWA1*, *METRNL*, and *HSPA1A* (Figure 3E). SIE-specific genes included *WNT9A*, *CCN1*, and *TIMP3* (Figure 3F), whereas MIE-specific genes included *APLN*, *FCN1*, and *MMP25* (Figure 3G).

While insightful, bulk RNA sequencing lacks cell-type resolution, preventing the identification of muscle fiber-derived secretory proteins. To address this limitation, we isolated and differentiated primary human skeletal muscle cells to determine whether secretory proteins predicted from bulk skeletal muscle transcriptomic data could be released by muscle fibers. For this, we used bio-orthogonal non-canonical amino acid tagging (BONCAT), a protein-labeling strategy in which a methionine analog, azidohomoalanine (AHA), is incorporated into the nascent cellular proteome and subsequently affinity purified via click chemistry for proteomic analysis.[30,31] Critically, this enrichment strategy detects proteins synthesized within cells, thereby circumventing the need for serum depletion. Using this approach, we detected hundreds of myotube-derived proteins, including low-abundance proteins such as myostatin (Figure S4C; Table S3). We then overlaid the myotube-derived proteins with the bulk skeletal muscle gene expression datasets. Of the original 170 genes predicted to encode secreted proteins (Figures 3E–3G), 46 were detected in the myotube-conditioned media (Table S3). These included SIE-regulated proteins (CCN1, TIMP3, and HSP90AB1), MIE-regulated proteins (VCAM1, KITLG, and STC1), and proteins shared across both exercise intensities (VEGFA, PLAU, FSTL3, METRNL, and ANGPTL4) (Figure S4C). Notably, an orthogonal Olink-based assay of conditioned media from human induced pluripotent stem cell (iPSC)-derived skeletal muscle cells identified many of the same proteins (39 of 170), further supporting the potential contribution of muscle fibers to their release (see STAR Methods; Table S3).

Finally, to determine whether the secretion of muscle fiber-derived proteins is intensity dependent, we electrically stimulated immortalized mouse myotubes (C2C12), using simulated SIE or MIE protocols (S-SIE and S-MIE, respectively), in combination with BONCAT protein labeling (see STAR Methods).[32] We used C2C12 cells because primary human muscle cells do not contract in the 2D culture system in response to electrical stimulation.[33] Consistent with the greater energetic demand imposed by S-SIE, this protocol increased phosphorylated AMPK (T172) relative to both S-MIE and control cells (Figures S4D and S4E). Following each stimulation protocol, proteins from the conditioned media were affinity purified via click chemistry and analyzed using liquid chromatography-tandem mass spectrometry (LC-MS/MS). PCA demonstrated a clear separation of samples by condition (Figure 3H), and differential analysis revealed more proteins released into the conditioned media following S-SIE than following S-MIE (212 versus 9 proteins; FDR < 0.1; Figure 3I). Of the S-SIE regulated proteins, 11 were also differentially regulated in the transcriptome of bulk human skeletal muscle, including CCN1, HSP90AB1, ANGPTL4, CCL2, LGALS1, and HSPA1A (Figure 3J). Of the S-MIE regulated proteins, two—ANGPTL4 and CCL2—were also differentially regulated in bulk skeletal muscle (Figure 3J). Notably, myotube-derived proteins following S-SIE positively correlated with the SIE plasma proteome at 0 h, whereas no such association was observed between S-MIE and the MIE plasma proteome. These findings suggest that skeletal muscle contributes to the systemic circulation in response to very-high-intensity exercise (Figures S4F–S4I). While inferential, these findings nonetheless suggest that exercise intensity shapes the release of organ-enriched proteins into the circulation, with skeletal muscle serving as a prime example of a tissue that contributes to the plasma proteome in an intensity-dependent manner.

Transcriptomic remodeling of adipocytes following SIE or MIE

Next, we sought to determine the cellular/tissue targets of these secretory proteins. To do so, we integrated a human receptor database from CellTalkDB that includes all known or predicted ligand-receptor pairs.[34] We filtered this list for organ-enriched receptors based on GTEx gene expression levels, as described above, and then queried our organ-enriched plasma protein dataset to identify ligands known or predicted to signal through any of the remaining organ-enriched receptors. This approach revealed multiple ligand-receptor (ligand:receptor) pairs differentially regulated immediately following acute SIE, including interactions with the brain (OMG:LINGO1), immune cells (ANXA1:FPR1), adrenals (POMC:MC2R), intestine (GUCA2A:GUCY2C), and kidney (PTH:PTH1R). Predicted crosstalk persisted, albeit to a lesser degree, 3 h following SIE, including with the brain (PENK:OPRK1), immune cells (IL1RN:IL1R2), and adrenals (POMC:MC2R) (Table S4). We did not identify any ligand-receptor pairs following MIE, likely reflecting our stringent inclusion criteria.

To more thoroughly characterize how exercised plasma signals to cells in an intensity-dependent manner, we conducted a media

Please cite this article in press as: Olsen et al., Exercise intensity modulates interorgan communication and is associated with cardiometabolic health outcomes in humans, Cell Reports Medicine (2026), https://doi.org/10.1016/j.xcrm.2026.102988

CellPress
OPEN ACCESS

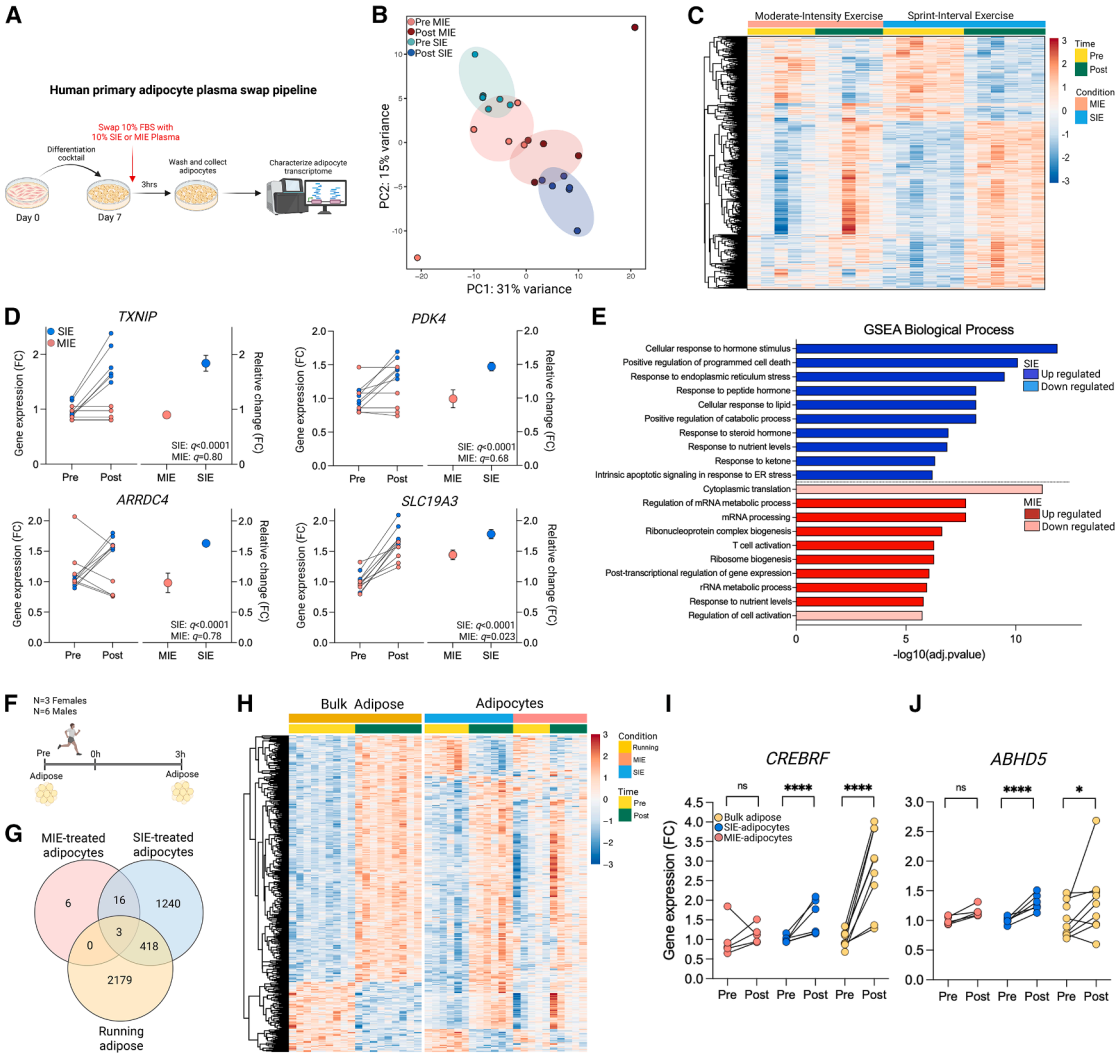

Figure 4. Transcriptomic remodeling of adipocytes following SIE or MIE

(A) Experimental design of the plasma swap with primary human adipocytes.

(B) Principal component analysis of the adipocyte transcriptome with "pre" or "0 h" plasma from SIE or MIE participants. $N = 5–6$ plasma samples from individual participants per intensity were used.

(C) A heatmap of all differentially expressed genes following SIE or MIE plasma treatment.

(D) Adipocyte genes of interest and their fold change, including individual values and mean fold change across groups, following incubation with SIE or MIE plasma.

(E) Gene set enrichment analysis (GSEA) of "biological pathways" for all detected genes ranked by the change in expression followed by SIE or MIE plasma-treated adipocytes.

(F) Exercise schematic of adipose tissue collected before (pre) and 3 hours (3 h) following a graded treadmill exercise test.

(G) Venn diagram of the DEGs from the plasma swap samples (C) and those following treadmill exercise.

(H–J) A heatmap of shared DEGs from (G). Fold change across conditions for *CREBRF* (I) and *ABHD5* (J). Error bars indicate standard error of the mean. $^{*}p < 0.05$, $^{****}p < 0.0001$. Statistical analysis for (I) and (J) is described in STAR Methods.

See also Figure S5.

swap experiment in primary human adipocytes, a cell type argued by some,[35–39] though not all,[40] to undergo metabolic remodeling according to exercise intensity. To interrogate this, we incubated differentiated human subcutaneous adipocytes for 3 h with plasma collected either before or immediately following SIE or MIE from 5–6 participants per exercise type, followed by bulk RNA sequencing (Figure 4A). PCA revealed intensity-dependent clustering of the adipocyte transcriptome, with SIE-treated adipocytes shifting along PC1 and MIE-treated adipocytes showing only a slight change (Figure 4B). This result was supported by robust transcriptomic changes observed for SIE-treated adipocytes, with 1,128 and 549 genes upregulated and downregulated, respectively, including metabolic regulators *TXNIP*, *PDK4*, and *ARRDC4* (FDR < 0.05; Figures 4C and 4D; Table S4). In contrast, MIE-treated

Please cite this article in press as: Olsen et al., Exercise intensity modulates interorgan communication and is associated with cardiometabolic health outcomes in humans, Cell Reports Medicine (2026), https://doi.org/10.1016/j.xcrm.2026.102988

adipocytes had 14 upregulated and 11 downregulated genes (FDR < 0.05; Figure 4C), most of which, such as *CISH*, *GLUL*, and *SLC19A3*, were also differentially expressed in SIE-treated adipocytes (Figure 4D).

Gene set enrichment analysis (GSEA) revealed multiple metabolic pathways enriched within SIE-treated adipocytes, including "cellular response to hormone stimulus," "positive regulation of catabolic process," and "response to nutrient levels" (Figure 4E). In contrast, MIE-treated adipocytes displayed enriched GSEA pathways controlling gene and protein expression; however, these data should not be overinterpreted given the low number of DEGs following MIE plasma treatment. Notably, an independent media swap experiment with an extended 12 h incubation period further supported the intensity-dependent shifts to the adipocyte transcriptome (Figures S5A–S5D; Table S4).

Despite these intriguing observations, high-intensity exercise has been shown to decrease adipose tissue blood flow, potentially diminishing acute exposure to the systemic circulation.[41] To confirm that the above-described findings persist within intact adipose tissue, we conducted a maximal graded treadmill exercise test in nine young, metabolically healthy male and female participants (mean age = 28 years; mean BMI = 26.4), and collected subcutaneous abdominal adipose tissue before and 3 h after exercise. We used treadmill exercise to maximize body-wide metabolic changes, specifically of adipose tissue[42] (Figure 4F). Bulk RNA sequencing of adipose tissue revealed clear exercise-dependent clustering (Figure S5E), with 2,600 genes differentially expressed 3 h following exercise (FDR < 0.05; Figure S5F; Table S4). The most significant DEGs following exercise were *HIPK3* and *ZBED6*, in addition to the well-described exercise-regulated genes *ANGPTL4* and *DICER1*. Pathway analysis of upregulated genes highlighted elevated cellular response to a hormone stimulus, in addition to multiple lipid biosynthesis signaling pathways (Figure S5G).

To identify shared DEGs within our *in vitro* and *in vivo* datasets—indicating cellular signaling driven, at least in part, by circulating factors—we overlaid the DEGs between SIE-treated adipocytes, MIE-treated adipocytes, and bulk adipose tissue (Figures 4G and 4H). As anticipated, most shared DEGs (418 genes) were between SIE-treated adipocytes and bulk human adipose tissue, including the fatty acid-handling genes *ABHD5* and *CREBRF* (Figures 4I and 4J). In fact, the phenotype classifier Mammalian Phenotype Ontology revealed "decreased body weight" and "decreased susceptibility to diet-induced obesity" as enriched within these shared genes (Table S4). In addition, several adipocyte receptors and their cognate ligands were expressed concordantly across transcriptomic and plasma proteomic datasets, most notably those in the IL-6 cytokine family (e.g., *IL6R* and *LIFR*), and showed greater expression following SIE. Taken together, our results point to exercise intensity as an important determinant of downstream tissue responsiveness, with adipose tissue providing an example of a target organ that responds selectively to the post-exercise plasma environment.

Identification of exercise-regulated proteins protective from cardiometabolic disease

Thus far, our findings support the conclusion that intensity-dependent effects on systemic metabolism are mediated, at least in part, by distinct exercise-induced secretomes that modulate interorgan communication. Although these responses are acute, the long-term cardiometabolic benefits of exercise arise from repeated bout of acute physical activity. Accordingly, recurrent exposure to transient increases in beneficial circulating proteins has been proposed to contribute to cardiometabolic adaptation.[43] Building on this concept, we asked whether plasma proteins acutely regulated by SIE or MIE are associated with future health or disease outcomes.

To address this, we leveraged a UK Biobank plasma proteome-phenome resource comprising 53,026 human participants and 1,066 incident and prevalent diseases.[44] Across the 741 exercise-regulated proteins, including those regulated by SIE and MIE, we identified 46,993 protein-disease associations (Bonferroni-adjusted $p < 0.05$; Figure 5A; Table S5). Most associations had hazard or odds ratios (HR/OR) greater than 1, consistent with prior literature showing that acute exercise induces a transient inflammatory and stress-response program.[45] While such acute inflammatory signals are important for adaptation to repeated exercise, as demonstrated for IL-6, we sought to prioritize proteins plausibly linked to cardiometabolic benefit and, therefore, focused on associations with an HR/OR of less than 1.

This approach identified 143 proteins spanning 14 disease chapters (Figure 5B), most of which were differentially regulated exclusively following SIE. Notably, the chapters "blood and blood forming organs," "endocrine, nutritional, and metabolic diseases," and "circulatory system" contained the greatest number of proteins with an HR/OR of <1 (Figure 5B). Many proteins were associated with a lower risk across multiple disease chapters, including CLEC3B (13 chapters); NELL1, FGFBP1, and OMG (12 chapters); ADGRG2, SDC4, and TNFSF11 (11 chapters); and ENPP6 (10 chapters). Over-representation analysis of the 143 proteins using Fisher's exact test revealed multiple pathways being significantly enriched, albeit nominally ($p < 0.05$), for immune regulation ("neutrophil mediated immunity") and blood metabolism ("plasminogen activation" and "negative regulation of blood coagulation") (Table S5).

Because each disease chapter contains multiple disorders, we next prioritized proteins associated with a lower risk of specific diseases of interest, namely metabolic disorders, obesity, and type 2 diabetes. This identified 33 proteins with varying effects across disease states (Figure 5C; Table S5). Nearly all of these proteins (32 of 33) were found to be differentially regulated following SIE at either 0 h (29 proteins) or 3 h (4 proteins; POMC is shared across time points) (Figure 5C). In contrast, MIE regulated three of the proteins—TNFSF11, FGF19, and FST. Notably, ADGRG2, FGFBP1, and MXRA8—all increasing immediately following SIE—consistently showed a low HR/OR across metabolic disease states. In fact, in a UK Biobank subgroup,[46] plasma levels of ADGRG2 and MXRA8 were positively associated with regular physical activity, suggesting that their potential benefit extends beyond the acute exercise window. To determine potential long-term intensity-dependent systemic benefits, we cross-referenced these 33 proteins with a large-scale plasma proteome association analysis of chronological aging. We found that more than a quarter were inversely associated with age, including IGDCC4, the protein with the strongest negative association with age[47] (Table S5). Overall, these data emphasize the

Please cite this article in press as: Olsen et al., Exercise intensity modulates interorgan communication and is associated with cardiometabolic health outcomes in humans, Cell Reports Medicine (2026), https://doi.org/10.1016/j.xcrm.2026.102988

CellPress
OPEN ACCESS

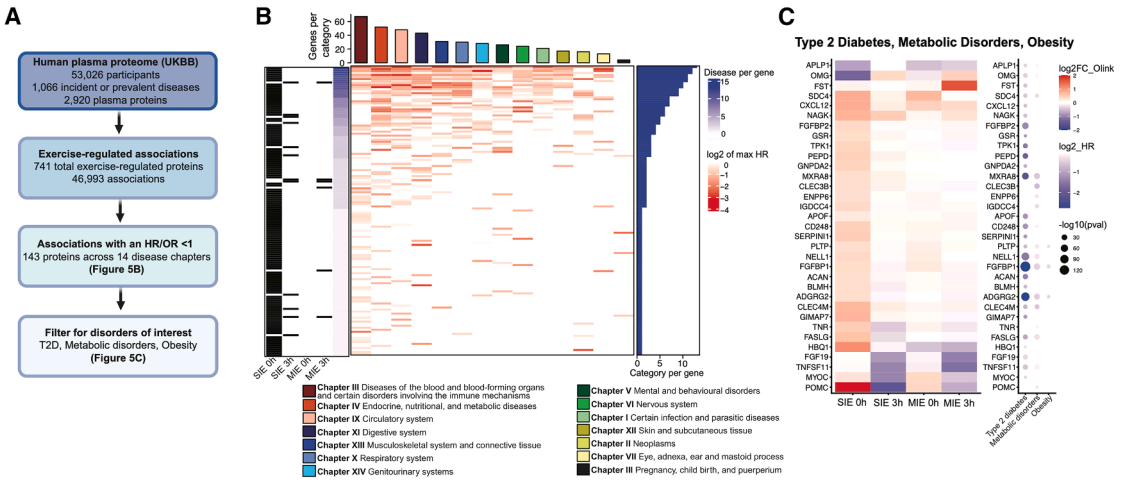

Figure 5. Identification of exercise-regulated proteins protective from cardiometabolic disease

(A) The workflow for the identification of proteins associated with and protective from cardiometabolic disease.

(B) A heatmap showing the 143 proteins with an HR/OR of less than 1 corresponding to their disease chapter. Whether a protein is significant (black) or non-significant (white) is shown on the far-left. The bar plot on the top shows how many gene are in a given category. How many categories are associated with a given gene is shown in the far-right.

(C) A heatmap of proteins protective from type 2 diabetes, metabolic disorders, or obesity. The heatmap corresponds to the protein $\log_2$FC relative to the "pre" time point. The bubble plot corresponds to the degree of protection ($\log_2$_hazard ratio) and significance ($-\log_{10}$pval).

coordinated, multi-system response to distinct exercise intensities and may offer clues into how short bursts of vigorous physical activity can elicit whole-body metabolic benefits.

DISCUSSION

SIE has increased in popularity because it requires relatively little time (3–5 min of total work) yet elicits marked whole-body adaptations. We reasoned that these intensity-dependent adaptations arise, at least in part, through circulating signals.[48] Using an antibody-based protein detection platform, we identified nearly 3,000 proteins across >100 plasma samples and observed marked intensity-dependent regulation. SIE altered ~25% of detected plasma proteins, including factors involved in angiogenesis (VWF), extracellular matrix remodeling (TIMP3), gut signaling (TFF2), and potential neuro-regulation (POMC). Plasma metabolomics similarly reflected the acute energetic demands of SIE, with lactate, pyruvate, and malate increasing immediately following exercise. Several acutely modulated metabolites may promote health benefits, including the obesity-mitigating metabolite Lac-Phe. In contrast, fatty acids displayed delayed release into the plasma, potentially reflecting a shift from carbohydrate toward lipid metabolism during recovery.

Although MIE produced only modest overall changes to the plasma proteome, the proteins that changed included well-described endocrine factors such as ANGPTL4, IGFBP1, and FST, with IGFBP1 and FST increasing exclusively after MIE. These responses may reflect the sustained energetic demands of continuous exercise, including an increased glucagon-to-insulin ratio and liver glycogen depletion, which stimulate hepatic secretion of FST and IGFBP1.[49–51] The liver, along with adipose tissue, may be particularly sensitive to exercise intensity and duration, as many of the most differentially regulated plasma proteins at 3 h are hepatokines.[50] The delayed increase in plasma proteins and fatty acids after MIE likely reflects both intensity-dependent and duration-dependent changes to the secretome, although our exercise paradigm could not separate these two variables.

A potentially underappreciated mode of exercise-induced cellular crosstalk, particularly following high-intensity exercise, is ectodomain shedding of transmembrane proteins. These proteolytically cleaved proteins contribute to the "sheddome,"[52] and regulate skeletal muscle, neural, and liver metabolism.[53–55] For example, the hepatokine syndecan-4 (SDC4) undergoes ectodomain shedding in response to exercise, thereby improving hepatic metabolic function.[55] While our Olink-based approach cannot distinguish between cleaved and full-length proteins—a similar challenge with POMC detection—the increased abundance of multiple metalloproteases supports the sheddome as a contributor to the exercise secretome.

The identification of intensity-dependent circulating proteins suggests dynamic interorgan crosstalk. Consistent with this, the release of many organ-enriched proteins into the circulation is acutely stimulated by SIE, as revealed by multi-tissue gene and protein expression resources[25,26]. We investigated this more directly by profiling skeletal muscle following SIE and MIE and assessing protein release from the primary human skeletal muscle cells and electrically stimulated C2C12 cells. Together, these datasets support the intensity-dependent release of muscle fiber-derived proteins, with SIE stimulating greater release of proteins, at least, *in vitro*. However, simulating SIE *in vitro* can increase cell damage and cytosolic protein release, representing a limitation of our EPS paradigm. Moreover, recent cell type-selective labeling detected minimal muscle fiber-derived proteins in the systemic circulation after exercise,[56] suggesting that muscle-derived proteins may preferentially

Please cite this article in press as: Olsen et al., Exercise intensity modulates interorgan communication and is associated with cardiometabolic health outcomes in humans, Cell Reports Medicine (2026), https://doi.org/10.1016/j.xcrm.2026.102988

signal locally within skeletal muscle.[57,58] Further work is needed to define their intensity-dependent contribution to the human systemic circulation.

The targets of exercise-regulated circulating proteins remain elusive. Our findings highlight adipocytes as an intensity-responsive target cell type. SIE plasma induced marked remodeling of the adipocyte transcriptome, and a subset of these changes were also present in human subcutaneous adipose tissue after exercise. For example, receptors of the IL-6 cytokine family (e.g., *IL6ST*, *IL6R*, and *LIFR*) were differentially expressed, while their ligands, most notably oncostatin M (OSM) and IL-6, increased in plasma. We previously found that OSM is a macrophage-derived ligand that signals to adipocytes following exercise.[59] While our data suggest intensity-dependent regulation of abdominal subcutaneous adipocytes, they do not address depot-specific responses, such as intermuscular adipocytes.[60–62] Future work should determine whether these responses persist across adipose tissue depots in humans.

Collectively, these findings demonstrate that the exercise intensity is a major determinant of the human secretome and drives distinct proteomic and metabolomic responses and differences in predicted tissues of origin and target tissues. Integration with a large plasma proteome-phenome repository suggests that SIE acutely stimulates the release of protective proteins into the circulation to a greater extent than MIE. These data help explain how SIE, despite requiring only a fraction of the time of MIE, elicits robust metabolic signaling and whole-body benefits.

Limitations of the study

Several limitations should be acknowledged, the most notable of which is the small and male-biased cohorts. Future work is needed to determine whether these findings are shared between sexes and to assess how intensity-dependent circulating factors influence systemic metabolism. Although we provide extensive datasets of intensity-dependent plasma metabolomics, we were unable to determine organ-of-origin or destination, an underdeveloped area in interorgan crosstalk that warrants future investigation.

RESOURCE AVAILABILITY

Lead contact

Requests for further information, resources, and reagents should be directed to and will be fulfilled by the lead contact, Paul Cohen (pcohen@rockefeller.edu).

Materials availability

This study did not generate new unique reagents.

Data and code availability

- RNA sequencing data generated in this study have been deposited in the Gene Expression Omnibus database (GEO: GSE308252). The MS proteomics data have been deposited to the ProteomeXchange Consortium via the PRIDE partner repository, with the dataset identifier PXD069170. The untargeted metabolomics data have been deposited in the Metabolomics Workbench under project ID PR002719.
- This paper does not report original code.
- Any additional information required to reanalyze the data reported in this work is available from the lead contact upon request.

ACKNOWLEDGMENTS

We would like to thank the Rockefeller University Hospital, including Lucy Apicello, Rita Devine, Lin Zhen, Regina Butler, Tia Gareau, Jill McCabe, and Andrea Ronning for their help with recruitment and on-site visits. We thank Richard Hutt, Rhonda Kost, Anna Rauso, Vanessa Smith, Dale Miller, Teresa Solomon, and Sarah Schlesinger for guidance with Institutional Review Board (IRB) submissions, clinical trial submissions, and contract agreements between institutions. We thank Connie Zhao and Bin Zhang from the Genomics Resource Center, and Wei Wang and Thomas Carroll of the Bioinformatics Resource Center for RNA sequencing, processing, and thoughtful discussions. We thank Elizabeth Zunica for organizing human sample shipments. We thank all participants who volunteered their time to take part in these studies. Figures were created in BioRender (https://BioRender.com). L.O. was supported by the Simons Foundation Postdoctoral Fellowship, the Harvey L. Karp Postdoctoral Fellowship, a BFTDF pilot award, pilot awards from the RUCCTS, and funding from the Nicholson Exchange Program. J.M.R. was supported by the NIH (R03 OD038387). P.C. and R.E.G. were supported by the Leducq Foundation for Cardiovascular Research (21CVD01). P.C. was also supported by the NIDDK (RC2 DK129961), and R.E.G was supported by R01 HL133870. This work was supported by the Clinical and Translational Science Awards (CTSA) grant UL1TR004419 from the National Center for Advancing Translational Sciences. J.R.Z was supported by grants from the European Research Council (ERC-2023-AdG 101142093) and Wallenberg Scholar grant from Knut and Alice Wallenberg Foundation (2023.0312). J.P.K. and C.L.A. were supported, in part, by The Louisiana Clinical and Translational Science (LA CaTS) Center (U54 GM104940). J.R.Z and A.K. were supported by the Strategic Research Programme in Diabetes at Karolinska Institutet (2009-1068) and the Swedish Research Council (2015-00165 and 2025-02427). A.K. holds a Distinguished Investigator Grant within Endocrinology and Metabolism from the Novo Nordisk Foundation (NNF24OC0088739). E.R. was supported by the Dr. Robert C. and Veronica Atkins Foundation. E.V.V and H.S. were supported by the Stavros Niarchos Foundation (SNF) as part of its grant to the SNF Institute for Global Infectious Disease Research at The Rockefeller University. E.V.V. was also supported by the Rockefeller University start-up funds, Robertson Foundation, The Achelis and Bodman Foundation, and Searle Scholars Program.

AUTHOR CONTRIBUTIONS

L.O. and P.C. conceptualized the study; L.O. and P.C. acquired funding; L.O. and D.B. analyzed and visualized data; L.O., J.B., D.J.B., and P.C. designed and interpreted experiments; L.O., J.B., L.Y., L.F., K.B., C.L.A., M.K., H.S., C.P., E.R., E.K., K.F., N.Z., and K.P. performed the experiments; J.W. collected human adipose tissue samples; P.C., D.J.B., L.O., J.B., A.K., J.R.Z., E.V.V., J.P.K., N.P., H.M., and O.P. supervised study/study segments; R.E.G., J.M.R., and O.P. provided technical and intellectual input; L.O. and P.C. wrote the manuscript. All authors read and approved the final version of the manuscript.

DECLARATION OF INTERESTS

P.C. is an advisor for Canary Cure Therapeutics, Hoxton Farms, Moonwalk Biosciences, and Cellular Intelligence; O.P. is a scientific co-founder and a shareholder of Cellular Intelligence; J.R.Z. is an Advisory Board member for Cell Metabolism.

DECLARATION OF GENERATIVE AI AND AI-ASSISTED TECHNOLOGIES IN THE WRITING PROCESS

This manuscript benefited from limited use of ChatGPT (OpenAI) to assist with initial grammatical editing and improving conciseness; all scientific content and interpretations were generated and verified by the authors.

STAR★METHODS

Detailed methods are provided in the online version of this paper and include the following:

SUPPLEMENTAL INFORMATION

Supplemental information can be found online at https://doi.org/10.1016/j.xcrm.2026.102988.

Received: October 20, 2025
Revised: May 18, 2026
Accepted: July 17, 2026

REFERENCES

1. Chow, L.S., Gerszten, R.E., Taylor, J.M., Pedersen, B.K., van Praag, H., Trappe, S., Febbraio, M.A., Galis, Z.S., Gao, Y., Haus, J.M., et al. (2022). Exerkines in health, resilience and disease. Nat. Rev. Endocrinol. *18*, 273–289. https://doi.org/10.1038/s41574-022-00641-2.
2. Robbins, J.M., and Gerszten, R.E. (2023). Exercise, exerkines, and cardiometabolic health: from individual players to a team sport. J. Clin. Investig. *133*, e168121. https://doi.org/10.1172/JCI168121.
3. Ahn, C., Zhang, T., Yang, G., Rode, T., Varshney, P., Ghayur, S.J., Chugh, O.K., Jiang, H., and Horowitz, J.F. (2024). Years of endurance exercise training remodel abdominal subcutaneous adipose tissue in adults with overweight or obesity. Nat. Metab. *6*, 1819–1836. https://doi.org/10.1038/s42255-024-01103-x.
4. Nigro, P., Vamvini, M., Yang, J., Caputo, T., Ho, L.L., Carbone, N.P., Papadopoulos, D., Conlin, R., He, J., Hirshman, M.F., et al. (2023). Exercise training remodels inguinal white adipose tissue through adaptations in innervation, vascularization, and the extracellular matrix. Cell Rep. *42*, 112392. https://doi.org/10.1016/j.celrep.2023.112392.
5. Stanford, K.I., Middelbeek, R.J.W., and Goodyear, L.J. (2015). Exercise Effects on White Adipose Tissue: Beiging and Metabolic Adaptations. Diabetes *64*, 2361–2368. https://doi.org/10.2337/db15-0227.
6. Richter, E.A., Ploug, T., and Galbo, H. (1985). Increased muscle glucose uptake after exercise. No need for insulin during exercise. Diabetes *34*, 1041–1048. https://doi.org/10.2337/diab.34.10.1041.
7. De Miguel, Z., Khoury, N., Betley, M.J., Lehallier, B., Willoughby, D., Olsson, N., Yang, A.C., Hahn, O., Lu, N., Vest, R.T., et al. (2021). Exercise plasma boosts memory and dampens brain inflammation via clusterin. Nature *600*, 494–499. https://doi.org/10.1038/s41586-021-04183-x.
8. Bishop, D.J., Lee, M.J.C., and Picard, M. (2025). Exercise as Mitochondrial Medicine: How Does the Exercise Prescription Affect Mitochondrial Adaptations to Training? Annu. Rev. Physiol. *87*, 107–129. https://doi.org/10.1146/annurev-physiol-022724-104836.
9. Morville, T., Sahl, R.E., Moritz, T., Helge, J.W., and Clemmensen, C. (2020). Plasma Metabolome Profiling of Resistance Exercise and Endurance Exercise in Humans. Cell Rep. *33*, 108554. https://doi.org/10.1016/j.celrep.2020.108554.
10. Guseh, J.S., Churchill, T.W., Yeri, A., Lo, C., Brown, M., Houstis, N.E., Aragam, K.G., Lieberman, D.E., Rosenzweig, A., and Baggish, A.L. (2020). An expanded repertoire of intensity-dependent exercise-responsive plasma proteins tied to loci of human disease risk. Sci. Rep. *10*, 10831. https://doi.org/10.1038/s41598-020-67669-0.
11. Li, V.L., He, Y., Contrepois, K., Liu, H., Kim, J.T., Wiggenhorn, A.L., Tanzo, J.T., Tung, A.S.H., Lyu, X., Zushin, P.J.H., et al. (2022). An exercise-inducible metabolite that suppresses feeding and obesity. Nature *606*, 785–790. https://doi.org/10.1038/s41586-022-04828-5.
12. Weber, D., Ferrario, P.G., and Bub, A. (2025). Exercise intensity determines circulating levels of Lac-Phe and other exerkines: a randomized crossover trial. Metabolomics *21*, 63. https://doi.org/10.1007/s11306-025-02260-0.
13. Helge, J.W., Stallknecht, B., Pedersen, B.K., Galbo, H., Kiens, B., and Richter, E.A. (2003). The effect of graded exercise on IL-6 release and glucose uptake in human skeletal muscle. J. Physiol. *546*, 299–305. https://doi.org/10.1113/jphysiol.2002.030437.
14. Pedersen, B.K., and Febbraio, M.A. (2008). Muscle as an endocrine organ: focus on muscle-derived interleukin-6. Physiol. Rev. *88*, 1379–1406. https://doi.org/10.1152/physrev.90100.2007.
15. Laurens, C., Parmar, A., Murphy, E., Carper, D., Lair, B., Maes, P., Vion, J., Boulet, N., Fontaine, C., Marquès, M., et al. (2020). Growth and differentiation factor 15 is secreted by skeletal muscle during exercise and promotes lipolysis in humans. JCI Insight *5*, e131870. https://doi.org/10.1172/jci.insight.131870.
16. Gillen, J.B., Martin, B.J., MacInnis, M.J., Skelly, L.E., Tarnopolsky, M.A., and Gibala, M.J. (2016). Twelve Weeks of Sprint Interval Training Improves Indices of Cardiometabolic Health Similar to Traditional Endurance Training despite a Five-Fold Lower Exercise Volume and Time Commitment. PLoS One *11*, e0154075. https://doi.org/10.1371/journal.pone.0154075.
17. Botella, J., Perri, E., Caruana, N.J., López-Calcerrada, S., Brischigliaro, M., Jamnick, N.A., Oorschot, V., Saner, N.J., Díaz-Lara, J., Taylor, D.F., et al. (2025). Sprint interval exercise disrupts mitochondrial ultrastructure driving a unique mitochondrial stress response and remodelling in men. Nat. Commun. *17*, 71. https://doi.org/10.1038/s41467-025-66625-8.
18. Zhong, W., Edfors, F., Gummesson, A., Bergström, G., Fagerberg, L., and Uhlén, M. (2021). Next generation plasma proteome profiling to monitor health and disease. Nat. Commun. *12*, 2493. https://doi.org/10.1038/s41467-021-22767-z.
19. Axelrod, C.L., Brennan, C.J., Cresci, G., Paul, D., Hull, M., Fealy, C.E., and Kirwan, J.P. (2019). UCC118 supplementation reduces exercise-induced gastrointestinal permeability and remodels the gut microbiome in healthy humans. Phys. Rep. *7*, e14276. https://doi.org/10.14814/phy2.14276.
20. Sato, S., Dyar, K.A., Treebak, J.T., Jepsen, S.L., Ehrlich, A.M., Ashcroft, S.P., Trost, K., Kunzke, T., Prade, V.M., Small, L., et al. (2022). Atlas of exercise metabolism reveals time-dependent signatures of metabolic homeostasis. Cell Metab. *34*, 329–345.e8. https://doi.org/10.1016/j.cmet.2021.12.016.
21. Roberts, L.D., Boström, P., O'Sullivan, J., Schinzel, R.T., Lewis, G.D., Dejam, A., Lee, Y.K., Palma, M.J., Calhoun, S., Georgiadi, A., et al. (2014). β-Aminoisobutyric acid induces browning of white fat and hepatic β-oxidation and is inversely correlated with cardiometabolic risk factors. Cell Metab. *19*, 96–108. https://doi.org/10.1016/j.cmet.2013.12.003.

22. Stanford, K.I., Lynes, M.D., Takahashi, H., Baer, L.A., Arts, P.J., May, F.J., Lehnig, A.C., Middelbeek, R.J.W., Richard, J.J., So, K., et al. (2018). 12,13-diHOME: An Exercise-Induced Lipokine that Increases Skeletal Muscle Fatty Acid Uptake. (2018). 12,13-diHOME: An Exercise-Induced Lipokine that Increases Skeletal Muscle Fatty Acid Uptake. Cell Metab. *27*, 1111–1120.e3. https://doi.org/10.1016/j.cmet.2018.03.020.

23. Agudelo, L.Z., Ferreira, D.M.S., Cervenka, I., Bryzgalova, G., Dadvar, S., Jannig, P.R., Pettersson-Klein, A.T., Lakshmikanth, T., Sustarsic, E.G., Porsmyr-Palmertz, M., et al. (2018). Kynurenic Acid and Gpr35 Regulate Adipose Tissue Energy Homeostasis and Inflammation. Cell Metab. *27*, 378–392.e5. https://doi.org/10.1016/j.cmet.2018.01.004.

24. GTEx Consortium (2020). The GTEx Consortium atlas of genetic regulatory effects across human tissues. Science *369*, 1318–1330. https://doi.org/10.1126/science.aaz1776.

25. Oh, H.S.H., Rutledge, J., Nachun, D., Pálovics, R., Abiose, O., Moran-Losada, P., Channappa, D., Urey, D.Y., Kim, K., Sung, Y.J., et al. (2023). Organ aging signatures in the plasma proteome track health and disease. Nature *624*, 164–172. https://doi.org/10.1038/s41586-023-06802-1.

26. Malmström, E., Malmström, L., Hauri, S., Mohanty, T., Scott, A., Karlsson, C., Gueto-Tettay, C., Åhrman, E., Nozohoor, S., Tingstedt, B., et al. (2025). Human proteome distribution atlas for tissue-specific plasma proteome dynamics. Cell *188*, 2810–2822.e16. https://doi.org/10.1016/j.cell.2025.03.013.

27. Zhu, W.G., Thomas, A.C.Q., Wilson, G.M., McGlory, C., Hibbert, J.E., Flynn, C.G., Sayed, R.K.A., Paez, H.G., Meinhold, M., Jorgenson, K.W., et al. (2025). Identification of a resistance-exercise-specific signalling pathway that drives skeletal muscle growth. Nat. Metab. *7*, 1404–1423. https://doi.org/10.1038/s42255-025-01298-7.

28. Severinsen, M.C.K., and Pedersen, B.K. (2020). Muscle-Organ Crosstalk: The Emerging Roles of Myokines. Endocr. Rev. *41*, 594–609. https://doi.org/10.1210/endrev/bnaa016.

29. Uhlén, M., Fagerberg, L., Hallström, B.M., Lindskog, C., Oksvold, P., Mardinoglu, A., Sivertsson, Å., Kampf, C., Sjöstedt, E., Asplund, A., et al. (2015). Proteomics. Tissue-based map of the human proteome. Science *347*, 1260419. https://doi.org/10.1126/science.1260419.

30. Dieterich, D.C., Link, A.J., Graumann, J., Tirrell, D.A., and Schuman, E.M. (2006). Selective identification of newly synthesized proteins in mammalian cells using bioorthogonal noncanonical amino acid tagging (BONCAT). Proc Natl Acad Sci USA *103*, 9482–9487. https://doi.org/10.1073/pnas.0601637103.

31. Choi, C.H.J., Barr, W., Zaman, S., Model, C., Park, A., Koenen, M., Lin, Z., Szwed, S.K., Marchildon, F., Crane, A., et al. (2022). LRG1 is an adipokine that promotes insulin sensitivity and suppresses inflammation. eLife *11*, e81559. https://doi.org/10.7554/eLife.81559.

32. Zanou, N., Dridi, H., Reiken, S., Imamura de Lima, T., Donnelly, C., De Marchi, U., Ferrini, M., Vidal, J., Sittenfeld, L., Feige, J.N., et al. (2021). Acute RyR1 Ca^{2+} leak enhances NADH-linked mitochondrial respiratory capacity. Nat. Commun. *12*, 7219. https://doi.org/10.1038/s41467-021-27422-1.

33. Olsson, K., Cheng, A.J., Alam, S., Al-Ameri, M., Rullman, E., Westerblad, H., Lanner, J.T., Bruton, J.D., and Gustafsson, T. (2015). Intracellular Ca(2+)-handling differs markedly between intact human muscle fibers and myotubes. Skeletal Muscle *5*, 26. https://doi.org/10.1186/s13395-015-0050-x.

34. Shao, X., Liao, J., Li, C., Lu, X., Cheng, J., and Fan, X. (2021). CellTalkDB: a manually curated database of ligand-receptor interactions in humans and mice. Briefings Bioinf. *22*, bbaa269. https://doi.org/10.1093/bib/bbaa269.

35. Lu, Z., Meng, C., Yang, J., Wang, X., Li, X., Zhang, J., Tian, X., and Wang, Q. (2025). Effect of different intensity aerobic exercise on remodeling immune microenvironment of adipose tissue in obesity mouse. Am. J. Physiol. Regul. Integr. Comp. Physiol. *328*, R220–R234. https://doi.org/10.1152/ajpregu.00227.2024.

36. Shirvani, H., and Arabzadeh, E. (2020). Metabolic cross-talk between skeletal muscle and adipose tissue in high-intensity interval training vs. moderate-intensity continuous training by regulation of PGC-1α. Eat. Weight Disord. *25*, 17–24. https://doi.org/10.1007/s40519-018-0491-4.

37. Sun, L., Li, F.H., Li, T., Min, Z., Yang, L.D., Gao, H.E., Wu, D.S., and Xie, T. (2020). Effects of high-intensity interval training on adipose tissue lipolysis, inflammation, and metabolomics in aged rats. Pflügers Archiv *472*, 245–258. https://doi.org/10.1007/s00424-020-02351-y.

38. Ahn, C., Zhang, T., Rode, T., Yang, G., Chugh, O.K., Ellis, S., Ghayur, S., Mehta, S., Salzman, R., Jiang, H., et al. (2025). Molecular responses in abdominal subcutaneous adipose tissue after a session of endurance exercise: effects of exercise intensity. J. Physiol. *603*, 6895–6919. https://doi.org/10.1113/JP289339.

39. Ahn, C., Jin, C.A., Whytock, K.L., Many, G.M., Sagendorf, T.J., Sanford, J.A., Hou, Z., Viggars, M.R., Nie, J., Espinoza, S.E., et al. (2026). Multiomic responses to acute exercise in abdominal subcutaneous adipose tissue of sedentary adults: Findings from MoTrPAC. Preprint at bioRxiv. https://doi.org/10.64898/2026.03.05.702363.

40. Ahn, C., Ryan, B.J., Schleh, M.W., Varshney, P., Ludzki, A.C., Gillen, J.B., Van Pelt, D.W., Pitchford, L.M., Howton, S.M., Rode, T., et al. (2022). Exercise training remodels subcutaneous adipose tissue in adults with obesity even without weight loss. J. Physiol. *600*, 2127–2146. https://doi.org/10.1113/JP282371.

41. Hodgetts, V., Coppack, S.W., Frayn, K.N., and Hockaday, T.D. (1991). Factors controlling fat mobilization from human subcutaneous adipose tissue during exercise. J. Appl. Physiol. (1985) *71*, 445–451. https://doi.org/10.1152/jappl.1991.71.2.445.

42. Chenevière, X., Malatesta, D., Gojanovic, B., and Borrani, F. (2010). Differences in whole-body fat oxidation kinetics between cycling and running. Eur. J. Appl. Physiol. *109*, 1037–1045. https://doi.org/10.1007/s00421-010-1443-5.

43. Robbins, J.M., Katz, D.H., Many, G.M., Rao, P., Smith, G.R., Tiwari, G., Jin, C., Spielmann, G., Montalvo, S., Iyer, G., et al. (2026). Blood Biochemical Responses to Acute Exercise: Findings from the Molecular Transducers of Physical Activity Consortium (MoTrPAC). Preprint at bioRxiv. https://doi.org/10.64898/2026.03.02.704798.

44. Deng, Y.T., You, J., He, Y., Zhang, Y., Li, H.Y., Wu, X.R., Cheng, J.Y., Guo, Y., Long, Z.W., Chen, Y.L., et al. (2025). Atlas of the plasma proteome in health and disease in 53,026 adults. Cell *188*, 253–271.e7. https://doi.org/10.1016/j.cell.2024.10.045.

45. Jurado-Fasoli, L., Di, X., Sanchez-Delgado, G., Yang, W., Osuna-Prieto, F.J., Ortiz-Alvarez, L., Krekels, E., Harms, A.C., Hankemeier, T., Schönke, M., et al. (2022). Acute and long-term exercise differently modulate plasma levels of oxylipins, endocannabinoids, and their analogues in young sedentary adults: A sub-study and secondary analyses from the ACTIBATE randomized controlled-trial. EBioMedicine *85*, 104313. https://doi.org/10.1016/j.ebiom.2022.104313.

46. Arani, G., Arora, A., Yang, S., Wu, J., Kraszewski, J.N., Martins, A., Miller, A., Zeba, Z., Jafri, A., Hu, C., et al. (2026). Plasma Proteomic Signatures of Physical Activity Provide Insights into Biological Impacts and its Protective Role against Dementia. Med. Sci. Sports Exerc. *58*, 1193–1206. https://doi.org/10.1249/MSS.0000000000003948.

47. Goeminne, L.J.E., Vladimirova, A., Eames, A., Tyshkovskiy, A., Argentieri, M.A., Ying, K., Moqri, M., and Gladyshev, V.N. (2025). Plasma protein-based organ-specific aging and mortality models unveil diseases as accelerated aging of organismal systems. Cell Metab. *37*, 205–222.e6. https://doi.org/10.1016/j.cmet.2024.10.005.

48. Ahn, C., Hevener, A.L., Goodyear, L.J., Bodine, S.C., Esser, K.A., Seldin, M.M., and Sparks, L.M. (2025). Exercise training remodels inter-organ endocrine networks. Mol. Metabol. *99*, 102219. https://doi.org/10.1016/j.molmet.2025.102219.

49. Hansen, J.S., Rutti, S., Arous, C., Clemmesen, J.O., Secher, N.H., Drescher, A., Gonelle-Gispert, C., Halban, P.A., Pedersen, B.K., Weigert, C., et al. (2016). Circulating Follistatin Is Liver-Derived and Regulated by the Glucagon-to-Insulin Ratio. J. Clin. Endocrinol. Metab. *101*, 550–560. https://doi.org/10.1210/jc.2015-3668.

50. Weigert, C., Hoene, M., and Plomgaard, P. (2019). Hepatokines-a novel group of exercise factors. Pflügers Archiv *471*, 383–396. https://doi.org/10.1007/s00424-018-2216-y.

51. Morville, T., Sahl, R.E., Trammell, S.A., Svenningsen, J.S., Gillum, M.P., Helge, J.W., and Clemmensen, C. (2018). Divergent effects of resistance and endurance exercise on plasma bile acids, FGF19, and FGF21 in humans. JCI Insight *3*, e122737. https://doi.org/10.1172/jci.insight.122737.

52. Huang, W.Y., and Wu, K.P. (2023). SheddomeDB 2023: A Revision of an Ectodomain Shedding Database Based on a Comprehensive Literature Review and Online Resources. J. Proteome Res. *22*, 2570–2576. https://doi.org/10.1021/acs.jproteome.3c00001.

53. Mori, S., Suzuki, S., Konishi, T., Kawaguchi, N., Kishi, M., Kuwabara, S., Ishizuchi, K., Zhou, H., Shibasaki, F., Tsumoto, H., et al. (2023). Proteolytic ectodomain shedding of muscle-specific tyrosine kinase in myasthenia gravis. Exp. Neurol. *361*, 114300. https://doi.org/10.1016/j.expneurol.2022.114300.

54. Martín-de-Saavedra, M.D., Santos, M.D., and Penzes, P. (2022). Intercellular signaling by ectodomain shedding at the synapse. Trends Neurosci. *45*, 483–498. https://doi.org/10.1016/j.tins.2022.03.004.

55. De Nardo, W., Miotto, P.M., Bayliss, J., Nie, S., Keenan, S.N., Montgomery, M.K., and Watt, M.J. (2022). Proteomic analysis reveals exercise training induced remodelling of hepatokine secretion and uncovers syndecan-4 as a regulator of hepatic lipid metabolism. Mol. Metabol. *60*, 101491. https://doi.org/10.1016/j.molmet.2022.101491.

56. Wei, W., Riley, N.M., Lyu, X., Shen, X., Guo, J., Raun, S.H., Zhao, M., Moya-Garzon, M.D., Basu, H., Sheng-Hwa Tung, A., et al. (2023). Organism-wide, cell-type-specific secretome mapping of exercise training in mice. Cell Metab. *35*, 1261–1279.e11. https://doi.org/10.1016/j.cmet.2023.04.011.

57. Stocks, B., Quesada, J.P., Mozzicato, A.M., Jacob, C., Jensen, S., MacGregor, K.A., Bangsbo, J., Zierath, J.R., Hostrup, M., and Deshmukh, A.S. (2025). Temporal dynamics of the interstitial fluid proteome in human skeletal muscle following exhaustive exercise. Sci. Adv. *11*, eadp8608. https://doi.org/10.1126/sciadv.adp8608.

58. Mittenbühler, M.J., Jedrychowski, M.P., Van Vranken, J.G., Sprenger, H.G., Wilensky, S., Dumesic, P.A., Sun, Y., Tartaglia, A., Bogoslavski, D., A, M., et al. (2023). Isolation of extracellular fluids reveals novel secreted bioactive proteins from muscle and fat tissues. Cell Metab. *35*, 535–549.e7. https://doi.org/10.1016/j.cmet.2022.12.014.

59. Dollet, L., Lundell, L.S., Chibalin, A.V., Pendergrast, L.A., Pillon, N.J., Lansbury, E.L., Elmastas, M., Frendo-Cumbo, S., Jalkanen, J., de Castro Barbosa, T., et al. (2024). Exercise-induced crosstalk between immune cells and adipocytes in humans: Role of oncostatin-M. Cell Rep. Med. *5*, 101348. https://doi.org/10.1016/j.xcrm.2023.101348.

60. Goodpaster, B.H., Bergman, B.C., Brennan, A.M., and Sparks, L.M. (2023). Intermuscular adipose tissue in metabolic disease. Nat. Rev. Endocrinol. *19*, 285–298. https://doi.org/10.1038/s41574-022-00784-2.

61. Kahn, D., Macias, E., Zarini, S., Garfield, A., Zemski Berry, K., Gerszten, R., Schoen, J., Cree-Green, M., and Bergman, B.C. (2022). Quantifying the inflammatory secretome of human intermuscular adipose tissue. Phys. Rep. *10*, e15424. https://doi.org/10.14814/phy2.15424.

62. Raajendiran, A., Krisp, C., Souza, D.P.D., Ooi, G., Burton, P.R., Taylor, R.A., Molloy, M.P., and Watt, M.J. (2021). Proteome analysis of human adipocytes identifies depot-specific heterogeneity at metabolic control points. Am. J. Physiol. Endocrinol. Metab. *320*, E1068–E1084. https://doi.org/10.1152/ajpendo.00473.2020.

63. Al-Khalili, L., Krämer, D., Wretenberg, P., and Krook, A. (2004). Human skeletal muscle cell differentiation is associated with changes in myogenic markers and enhanced insulin-mediated MAPK and PKB phosphorylation. Acta Physiol. Scand. *180*, 395–403. https://doi.org/10.1111/j.1365-201X.2004.01259.x.

64. Katz, D.H., Robbins, J.M., Deng, S., Tahir, U.A., Bick, A.G., Pampana, A., Yu, Z., Ngo, D., Benson, M.D., Chen, Z.Z., et al. (2022). Proteomic profiling platforms head to head: Leveraging genetics and clinical traits to compare aptamer- and antibody-based methods. Sci. Adv. *8*, eabm5164. https://doi.org/10.1126/sciadv.abm5164.

65. Assarsson, E., Lundberg, M., Holmquist, G., Björkesten, J., Thorsen, S.B., Ekman, D., Eriksson, A., Rennel Dickens, E., Ohlsson, S., Edfeldt, G., et al. (2014). Homogenous 96-plex PEA immunoassay exhibiting high sensitivity, specificity, and excellent scalability. PLoS One *9*, e95192. https://doi.org/10.1371/journal.pone.0095192.

66. Alis, R., Sanchis-Gomar, F., Primo-Carrau, C., Lozano-Calve, S., Dipalo, M., Aloe, R., Blesa, J.R., Romagnoli, M., and Lippi, G. (2015). Hemoconcentration induced by exercise: Revisiting the Dill and Costill equation. Scand. J. Med. Sci. Sports *25*, e630–e637. https://doi.org/10.1111/sms.12393.

67. Schrimpe-Rutledge, A.C., Codreanu, S.G., Sherrod, S.D., and McLean, J.A. (2016). Untargeted Metabolomics Strategies-Challenges and Emerging Directions. J. Am. Soc. Mass Spectrom. *27*, 1897–1905. https://doi.org/10.1007/s13361-016-1469-y.

68. Kolde, R. (2019). Pheatmap: Pretty Heatymaps. R package versision 1.0.12. https://doi.org/10.32614/CRAN.package.pheatmap.

69. Anim, E.P., Mezzanotte, J., Chu, S., and Stochaj, U. (2025). Bioorthogonal Non-Canonical Amino Acid Tagging (BONCAT) to detect newly synthesized proteins in cells and their secretome. PLoS One *20*, e0329857. https://doi.org/10.1371/journal.pone.0329857.

70. Seale, P., Bjork, B., Yang, W., Kajimura, S., Chin, S., Kuang, S., Scimè, A., Devarakonda, S., Conroe, H.M., Erdjument-Bromage, H., et al. (2008). PRDM16 controls a brown fat/skeletal muscle switch. Nature *454*, 961–967. https://doi.org/10.1038/nature07182.

71. Rao, J., Djeffal, Y., Chal, J., Marchianò, F., Wang, C.H., Al Tanoury, Z., Gapon, S., Mayeuf-Louchart, A., Glass, I., Sefton, E.M., et al. (2023). Reconstructing human brown fat developmental trajectory in vitro. Dev. Cell *58*, 2359–2375.e8. https://doi.org/10.1016/j.devcel.2023.08.001.

72. Chal, J., Al Tanoury, Z., Hestin, M., Gobert, B., Aivio, S., Hick, A., Cherrier, T., Nesmith, A.P., Parker, K.K., and Pourquié, O. (2016). Generation of human muscle fibers and satellite-like cells from human pluripotent stem cells in vitro. Nat. Protoc. *11*, 1833–1850. https://doi.org/10.1038/nprot.2016.110.

73. Plucińska, K., Chen, Z.Z., Xiang, R., Zaman, S., Yan, L., Hurson, C., Peterson, C., Fredrickson, K., Farrell, L., Walker, J., et al. (2025). Acute cold exposure in humans shifts the circulating proteome to a cardioprotective and anti-aging profile. Preprint at bioRxiv. https://doi.org/10.1101/2025.06.30.662436.

74. Patro, R., Duggal, G., Love, M.I., Irizarry, R.A., and Kingsford, C. (2017). Salmon provides fast and bias-aware quantification of transcript expression. Nat. Methods *14*, 417–419. https://doi.org/10.1038/nmeth.4197.

75. Soneson, C., Love, M.I., and Robinson, M.D. (2015). Differential analyses for RNA-seq: transcript-level estimates improve gene-level inferences. F1000Res. *4*, 1521. https://doi.org/10.12688/f1000research.7563.2.

76. Love, M.I., Huber, W., and Anders, S. (2014). Moderated estimation of fold change and dispersion for RNA-seq data with DESeq2. Genome Biol. *15*, 550. https://doi.org/10.1186/s13059-014-0550-8.

77. Subramanian, A., Tamayo, P., Mootha, V.K., Mukherjee, S., Ebert, B.L., Gillette, M.A., Paulovich, A., Pomeroy, S.L., Golub, T.R., Lander, E.S., and Mesirov, J.P. (2005). Gene set enrichment analysis: a knowledge-based approach for interpreting genome-wide expression profiles. Proc Natl Acad Sci USA *102*, 15545–15550. https://doi.org/10.1073/pnas.0506580102.

78. Yu, G., Wang, L.G., Han, Y., and He, Q.Y. (2012). clusterProfiler: an R package for comparing biological themes among gene clusters. OMICS *16*, 284–287. https://doi.org/10.1089/omi.2011.0118.

79. Dolgalev, I. (2025). Msigdbr: MSigDB Gene Sets for Multiple Organisms in a Tidy Data Format. R package version 25.1.1. https://doi.org/10.32614/CRAN.package.msigdbr.

Please cite this article in press as: Olsen et al., Exercise intensity modulates interorgan communication and is associated with cardiometabolic health outcomes in humans, Cell Reports Medicine (2026), https://doi.org/10.1016/j.xcrm.2026.102988

STAR★METHODS

KEY RESOURCES TABLE

REAGENT or RESOURCE	SOURCE	IDENTIFIER
Antibodies		
Phospho-AMPK alpha (Thr172) antibody	Cell Signaling Technology	Cat#2535;RRID:AB_331250
AMPK alpha antibody	Cell Signaling Technology	Cat#2793;RRID:AB_915794
IRDye 680-conjugated goat anti-mouse secondary antibody	LICOR	Cat#926-68070;RRID: AB_10956588
IRDye 800-conjugated goat anti-rabbit IgG	LICOR	Cat#926-32211;RRID: AB_621843
Biological samples		
Human plasma samples, exercise Cohort 1	Botella et al.[17]	Clinical trial ACTRN12617001105336
Human plasma samples, exercise Cohort 2	Axelrod et al.[19]	IRB #15-1311
Human subcutaneous abdominal adipose tissue, Cohort 3	Rockefeller University Hospital	IRB: LOL1044; Clinical trial ID: NCT06223035
Human primary myoblasts	Al-Khalili et al.[63]	N/A
Human subcutaneous preadipocytes	Lonza	Cat#PT-5001; Lots: 24TL271510, 25TL121766
Chemicals, peptides, and recombinant proteins		
L-Azidohomoalanine (AHA)	Click Chemistry Tools	Cat#1066
L-Methionine (MET)	Sigma	Cat#M5308
Lys-C	FUJIFILM Wako Chemicals	Cat#129-02541
Trypsin	Promega	Cat#V5111
Trifluoroacetic acid	Thermo Scientific	Cat#85183
Acetonitrile	Fisher Scientific	Cat#A955
Methanol	Fisher Scientific	Cat#A412
Formic acid	Fisher Scientific	Cat#A1171
Urea	Cytiva	Cat#17131901
Iodoacetamide	Sigma Aldrich	Cat#I1149
L-cystine	Sigma Aldrich	Cat#C7602
Dithiothreitol	Fisher Scientific	Cat#BP172-25
Acetone	Sigma Aldrich	Cat#179973
Critical commercial assays		
Olink Explore 3072 panel	Olink Proteomics AB	https://www.olink.com/explore
High-Select Top14 Abundant Protein Depletion Resin	Thermo Scientific	Cat#A36370
Calcium Colorimetric Assay Kit	Abcam	Cat#ab102505
Click-iT Protein Enrichment Kit	Invitrogen	Cat#C10416
Pierce BCA Protein Assay Kit	Thermo Scientific	Cat#23225
Illumina stranded mRNA kit	Illumina	Cat#20040534
RNeasy Plus Micro Kit	Qiagen	Cat#74034
PGM-2 Preadipocyte Growth Medium-2 BulletKit	Lonza	Cat#PT-8002
Deposited data		
All original RNA-sequencing data in this manuscript has been deposited in the Gene Expression Omnibus database	This paper	GEO: GSE308252
The mass spectrometry proteomics data have been deposited to the ProteomeXchange Consortium	This paper	PRIDE: PXD069170

(*Continued on next page*)

Continued

REAGENT or RESOURCE	SOURCE	IDENTIFIER
The untargeted metabolomics data have been deposited in the Metabolomics Workbench	This paper	Project ID: PR002719
Software and algorithms		
Spectronaut	Biognosys	Version 19
Compound Discoverer	Thermo Fisher Scientific	Version 3.3.2.31
DEP R Bioconductor package	Bioconductor	Version 1.26.0
limma R Bioconductor package	Bioconductor	Version 3.60.4
pheatmap R package	R package/CRAN	Version 1.0.12
NextSeq Control Software	Illumina	Version 1.7.1.46395
Salmon	Salmon	Version 1.8.0
tximport R Bioconductor package	Bioconductor	Version 1.22.0
DESeq2 R Bioconductor package	Bioconductor	Versions 1.42.1 and 1.44.0
clusterProfiler R Bioconductor package	Bioconductor	Version 4.12.6
msigdbr R package	R package/MSigDB interface	Version 25.1.1
Image Studio	LI-COR	Version 6.1
MaxQuant	Cox and Mann, 2008	Version 2.6.6.0
Other		
Illumina NovaSeq 6000	Illumina	Model: NovaSeq 6000
Tribrid Orbitrap Fusion ASCEND	Thermo Fisher Scientific	Model: Orbitrap Fusion ASCEND
IQ-X Orbitrap mass spectrometer	Thermo Fisher Scientific	Model: IQ-X Orbitrap
Vanquish UPLC System	Thermo Fisher Scientific	Model: Vanquish UPLC
Orbitrap Fusion LUMOS	Thermo Fisher Scientific	Model: Orbitrap Fusion LUMOS
Easy-nLC 1200 system	Thermo Fisher Scientific	Model: Easy-nLC 1200
C-Pace EM stimulator	IONOPTIX LLC	Model: C-Pace EM
IR-Odyssey/Fc infrared imaging system	LI-COR	Model: IR-Odyssey/Fc
Illumina NextSeq 2000	Illumina	Model: NextSeq 2000

EXPERIMENTAL MODEL AND STUDY PARTICIPANT DETAILS

Participant characterization and sample collection

Cohort 1

Plasma samples were obtained from Botella et al. 2024.[17] Ethical approval was obtained from the Victoria University Human Research Ethics Committee (HRE17-075) and registered as clinical trial ANZCTR; ACTRN12617001105336. All participants provided their written consent. Of the original 28 participants recruited, 19 were used for this study due to sample availability. Detailed methods for the exercise intervention and sample collection can be found in Botella et al. 2025.[17] Body composition and physical fitness metrics can be found in Table S6. In brief, 28 healthy males volunteered to participate in acute exercise testing before and after an 8-week training intervention (mean age: 26 years). Participants were matched based on their pre-determined maximum aerobic power followed by random assignment to either sprint-interval exercise or moderate-intensity exercise. Participants were provided a balanced set of meals 24 h prior to performing a single exercise session. The sprint-interval exercise session consisted of six, 30-s all-out cycling bouts against a resistance set at 0.075 kg · kg BM-1, interspersed by 4-min recovery periods. Sprint-interval training comprised 3–4 sprint-interval exercise sessions per week, with the resistance gradually increasing from 0.075 kg · kg BM-1 to 0.090 kg · kg BM-1 at week seven. Exercise sessions increased to eight sprints per session by week seven. The moderate-intensity exercise session consisted of continuous cycling at a fixed power equivalent to ~90 to 100% of the pre-determined first lactate threshold for 90 min. Moderate-intensity training consisted of progressively increasing exercise duration to 120 min per session in week seven, with the intensity adjusted based on submaximal tests performed every two weeks. Blood samples were collected before, immediately following, and 3 h following the single exercise sessions in the untrained and trained state.

Cohort 2

Plasma samples were obtained from Axelrod et al. 2019[19] (IRB#: 15–1311) with detailed methods described in the original publication. All participants provided their written consent. Participant characterization can be found in Table S6. In brief, this study included nine active, young, trained male and female participants ($N = 7$ and $N = 2$, respectively). Age information was available for 7 of the 9

participants from this cohort; the mean age of these 7 participants was 31 years. Participants arrived for testing in a fasted state at 0600, and received a standardized meal one hour prior to exercise testing. Exercise consisted of two hours of continuous running on a motorized treadmill at 60% of their pre-determined VO_{2max}. Blood was collected before and immediately following exercise.

Cohort 3

This study was approved by the Rockefeller University Institutional Review Board and registered as a clinical trial (IRB #: LOL1044; Clinical trial ID: NCT06223035). A total of eleven healthy, moderately active participants ($N = 7$ males; $N = 4$ females) were recruited to the Rockefeller University Hospital, provided their written consent, and completed all study sessions. The protocol consisted of two in-person visits. Visit one consisted of participants arriving at the hospital in the morning (0800–1000). All participants were asked to eat their regular breakfast at least two hours before arriving to the hospital. Body composition measurements were taken using air displacement plethysmography (BodPod; COSMED), and blood draws were taken from the median cubital vein and collected in K2 EDTA-coated tubes for clinical blood work. Following blood collection, participants were prepped for subcutaneous adipose collection from the lower abdomen. The area for tissue collection was numbed with a local anesthetic (lidocaine) and ~50 mg of adipose tissue was collected using a 6 mm punch biopsy needle. Skin and connective tissue was carefully removed and tissue was blotted for blood. Adipose samples were then immediately frozen in liquid nitrogen and stored at −80°C for future use.

Following a minimum of one week from adipose sample collection, participants arrived in the morning (0800–1000) to the Sports Rehabilitation and Performance Center at the Hospital for Special Surgery (HSS) for VO_{2max} testing. Participants were asked to consume the same breakfast as they did prior to visit one, at least two hours before arriving to HSS. Following familiarization with the protocol and equipment, participants underwent a five-minute warm up, comprising walking on a treadmill at a slow pace. Following five minutes, participants began the graded exercise test (GXT) which included a progressive increase in running speed and treadmill incline until participants reached volitional fatigue as defined by either reaching a rate of perceived exertion (RPE) greater than 19 (using the Borg RPE Scale), a respiratory exchange ratio (RER) reaching above 1.1, or if the participant chose to stop the test for any reason. The protocol used for the GXT, including speed, incline, and stage duration, can be found in Table S7. Blood lactate levels were measured before and immediately following exercise via a finger stick. Immediately following the exercise test, participants returned to the Rockefeller University Hospital for subsequent blood and adipose collection. Three hours following the exercise test, participants were prepped for abdominal subcutaneous adipose collection as described above. The opposite side of the abdomen (left or right of the navel from which the first biopsy was collected) was used for the second adipose collection. Upon collection, adipose was cleared of remaining skin and connective tissue, blotted for blood, and rapidly frozen. One male participant chose not to complete the second adipose biopsy and was thus not included. Additionally, the adipose sample from one female participant became compromised due to accidental exposure to room temperature and was not included. The final sample size for RNA sequencing was $N = 9$ ($N = 6$ males; $N = 3$ females; Mean age: 28 years; Table S6). Frozen adipose tissue was homogenized in a bead beater with Trizol (ThermoFisher Scientific: 15596026). RNA was separated via the Trizol-chloroform method. The subsequent RNA fraction was combined with 70% ethanol, which was then processed with the Qiagen RNeasy Plus Micro Kit (Qiagen: 74034), including DNAse incubation treatment. High-quality RNA was processed for RNA-sequencing as described in the RNA-sequencing section.

METHOD DETAILS

Sample processing for plasma OLINK proteomics

Plasma samples from Cohort 1 and Cohort 2 underwent proteomic profiling in a single batch using Olink Explore 3072 panel (Olink Proteomics AB, Uppsala, Sweden) according to the manufacturer's instructions; a detailed description of methods can be found elsewhere.[64] In brief, the Olink protocol is based on Proximity Extension Assay (PEA),[65] coupled with readout via next-generation sequencing (NGS) and enables the detection of ~3,000 proteins within a given biological sample. Specifically, pairs of oligonucleotide-labeled antibodies bind to their target protein, followed by nucleotide hybridization, polymerization, extension, and amplification using NGS Illumina NovaSeq 6000. The raw data output is quality controlled, normalized, and converted into NPX values, Olink's proprietary unit of relative abundance. All assay validation data (detection limits, intra- and inter-assay precision data) are available on manufacturer's website (www.olink.com/explore).

Sample processing for depleted plasma proteomics

Plasma samples from the untrained participants in Cohort 1 underwent depletion of abundant circulating proteins to improve detection of medium and low abundance proteins. Three participants were excluded due to insufficient plasma volume or poor quality. The remaining 16 participants (SIE = 8; MIE = 8; 48 plasma samples in total) underwent depletion using the High-Select Top14 Abundant Protein Depletion Resin (ThermoScientific, catalog # A36370). In brief, 6 μL of plasma per sample was added to the depletion resin, which was then rotated end-over-end for 15 min at room temperature (RT). The resin was subsequently spun down for two minutes at 1,000 g RT and the supernatant was collected. The collected supernatant was rapidly frozen in LN2 and placed at −80°C until follow-up proteomic analysis.

Depleted plasma samples were reduced (10mM Dithiothreitol) and alkylated (100mM Iodoacetamide) before undergoing overnight ice-cold acetone precipitation. Acetone was removed and pellets were dried in a speedvac, re-dissolved in 8 M urea, and subsequently sonicated for 10 min to dissolve large pellets. Samples were then digested via LysC (FUJIFILM Wako) for 6 h and trypsin

(Promega) overnight at <4 M urea and <2 M urea, respectively. Peptides were solid phase extracted and analyzed by LC-MS/MS using Thermo Scientific Tribrid Orbitrap Fusion ASCEND coupled to a Thermo Scientific *Neo* Vanquish system with a direct loading setup. Peptides were separated on a 25cm/75μm EASY Sprayer column (ThermoFisher, Catalog # ES902) using a 60-min analytical gradient (BufferA:Buffer B composition being 1% acetonitrile,0.1% formic acid: 80% acetonitrile, 0.1% formic acid, with a %B gradient of 1–37% at 350 nL/min). The instrument was operated in high-resolution/high-mass-accuracy DIA (Data Independent Acquisition) mode with optimized acquisition parameters. Raw files of the samples were analyzed by Spectronaut (v.19; Biognosys), where the data was searched as Direct-DIA (DIA files analyzed directly without the assist of a library) and underwent cross-run normalization, queued against the human database, concatenated with contamination sequences.

Serum calcium measurement and plasma volume correction

Serum calcium was used as an indirect proxy to assess changes to plasma volume.[66] Plasma samples were not used due to the incompatibility of plasma collection (EDTA-coated tubes) which interfere with calcium concentrations. In brief, all serum samples from Cohort 1 were measured for calcium concentration using a commercially available colorimetric assay (Abcam; catalog # ab102505). Serum samples were first diluted 5-fold and then further processed following the manufacturer's instructions. To correct plasma protein values for changes in calcium levels, we used the equation described previously,[38] specifically: [protein NPX value]c = [protein NPX value]u/(1+ ΔCa(%)/100). "ΔCa(%)" is the percent change of calcium concentration relative to pre-exercise, "c" is the corrected NPX (Olink) value, and "u" is the uncorrected NPX (Olink) value. Raw serum calcium values can be found in Table S1.

Sample processing for plasma untargeted metabolomics

Samples (20 μL) were extracted with 80 μL of 75:25:0.2 ACN:MeOH:FA extraction solution containing 1 μM heavy amino acid mix. After vortexing and centrifuging (at 13,200 rpm and 4°C for 15 min), 40 μL supernatant was transferred to HPLC vials. The remaining supernatants were combined to prepare a pooled QC sample to monitor for instrument variability such as mass error, chromatographic shift, and internal standard signal. Samples were analyzed using LC-MS on an IQ-X Orbitrap mass spectrometer coupled with a Vanquish UPLC System (ThermoFisher Scientific). For chromatographic separation, samples were loaded on a SeQuant ZIC-pHILIC column (150 × 2.1 mm, 5 μm polymeric) and a SeQuant ZIC-pHILIC Guard Kit (20 × 2.1 mm) at 40°C and eluted with a solvent system composed of mobile phase A (20 mM ammonium carbonate and 0.1% ammonium hydroxide in water at pH 9.3) and mobile phase B (100% acetonitrile). The injection volume was set to 5 μL, and samples were maintained at 4°C. The gradient (vol/vol) used was as follows: 0–22 min, linear gradient from 90% to 40% B; 22–24 min, held at 40% B; 24–24.1 min, returned to 90% B; 24.1–30 min, equilibrated at 90% B at a flow rate of 150 μL/min. Mass spectrometry was operated in polarity-switching mode for MS1 acquisition with the following source conditions: spray voltage, +3 kV and −2.5 kV; sheath gas, 40 AU; auxiliary gas, 15 AU; ion-transfer tube temperature, and probe heater temperature, 300°C. Samples were analyzed with the following acquisition parameters. MS1 scans: resolution, 120,000; AGC target, 1.2×10^5; maximum injection time, 246 ms; m/z ranges, 55–275 Th and 265–1000 Th. The pooled QC sample was analyzed using data-dependent acquisition method. Data-dependent MS/MS scans were acquired separately for each polarity (positive and negative) and mass range (55–275 Th and 265–1000 Th) using the following settings: a resolution of 15,000, 7.5e4 AGC target, auto max injection time mode, 1 Da isolation width, HCD activation, assisted normalized collision energy of 20, 30, 40 units, and a cycle time of 3 s. The instrument was externally calibrated weekly using Pierce FlexMix Calibration Solution (ThermoFisher Scientific) and the internal calibration feature (RunStart EASY-IC) was turned on.

The untargeted metabolomics analysis was conducted using Compound Discoverer 3.3.2.31 for identification and quantification. Data were filtered for MS2 library matches, retaining only compounds with a match score of ≥70 from either mzCloud (https://www.mzcloud.org/) or the MassBank of North America (https://mona.fiehnlab.ucdavis.edu/) via mzVault. These are referred to as annotated data, while all other detected features are considered unannotated. As metabolite annotation is a critical step that connects acquired analytical data to biologically meaningful insights, there are levels of confidence for metabolite identification depending on the amount of supporting metadata available. Metabolite identification confidence ranges from Level 5 (lowest) to Level 1 (highest): Level 5 is based solely on an exact mass measurement of a unique feature, allowing database searching but providing limited certainty; Level 4 improves mass accuracy, enabling assignment to a unique molecular formula, though multiple isomers may still be possible; Level 3 allows a tentative structure to be proposed by matching precursor m/z values to MS1 metabolite databases (i.e., ChemSpider, HMDB); Level 2 (putative identification) requires fragmentation spectra that match reference MS/MS libraries; and Level 1 (highest confidence) is achieved when fragmentation data and additional orthogonal evidence such as LC retention time match a reference standard under identical experimental conditions.[67] In this paper, emphasis is placed on features corresponding to Level 1 identifications (lactate, pyruvate, succinate, kynurenic acid, β-hydroxybutyrate, C12-carnitine, inosine, and malate), and Level 2 identifications (Lac-Phe, acetate, oleic acid, eicosadienoic acid, 7-hydroxylauric acid, 3α,7α-dihydroxycholanoic acid, and linoleic acid) to enhance the reliability of the findings. Using the same untargeted metabolomics dataset processed in Compound Discoverer, Lac-Phe was relatively quantified between groups of untrained participants via targeted analysis in Skyline. Structural annotation was confirmed by matching the precursor ion and MS/MS fragment ions to the mzCloud library (Thermo Fisher Scientific) reference spectrum (Table S2).

Please cite this article in press as: Olsen et al., Exercise intensity modulates interorgan communication and is associated with cardiometabolic health outcomes in humans, Cell Reports Medicine (2026), https://doi.org/10.1016/j.xcrm.2026.102988

Differential analysis of the olink plasma proteome and untargeted metabolites

For the proteome, the mean Olink NPX value for each protein was calculated and missing values were imputed using the DEP R Bioconductor package (v1.26.0). Specifically, imputation was done with the impute function with the 'knn' function and the 'rowmax' parameter set to 0.9. For both the proteome and metabolome, differential abundance between time points within each mode of exercise (sprint interval vs. moderate) was determined using the limma R Bioconductor package (v3.60.4). The correlation of abundance from the same participant across time points was estimated using the duplicateCorrelation function from limma, and this was included in the linear model fitting function (lmFit) with the 'block' parameter when comparing time points within each mode of intensity. Moderated t-statistics were obtained using empirical Bayes, and the topTable functions implemented within limma was used to identify all proteins that changed across the various timepoints for either mode of intensity after adjusting *p*-values with the Benjamini–Hochberg procedure. Adjustment for participant effects for visualization was performed using the removeBatchEffect function in limma. The z-scores of these participant-corrected abundance values for differential proteins or differential metabolites was visualized using the pheatmap R package (1.0.12).[68] Additionally, for Figure 2D, metabolite clustering was performed jointly across the full dataset so that shared and divergent temporal patterns could be compared on the same scale.

Azide-tagging of nascent secreted proteins in primary human muscle cells

Human primary myoblasts were obtained from muscle biopsies taken from the *vastus lateralis* of healthy volunteers, and have been previously authenticated.[63] Cells were left to proliferate in growth media consisting of DMEM/F12+Glutamax (Gibco: 31331), 1% Antibiotic-Antimycotic (Anti-anti) (Gibco: 15240–062), and 16% FBS (Sigma: F7524). Upon confluence, cells were differentiated in media consisting of DMEM (Gibco: 31966–021), 20% Medium 199 (Gibco: 31150–022), 2% HEPES (Gibco: 15630–056), 1% Anti-anti, 0.03 μg/mL Zinc sulfate (Sigma: Z4750), 1.4 μg/mL Vitamin B12 (Sigma: V6629), 2% FBS, 10 μg/mL insulin, and 100 μg/mL apo-transferrin (BBI Solutions: T100-5). Once fully differentiated (minimum of 75% differentiation), cells were washed with warmed PBS and provided fresh DMEM and differentiation cocktail with dialyzed FBS containing either azidohomoalanine (AHA, 0.1 mM; Click Chemistry Tools: 1066) or Methionine (MET, 0.1 mM; Sigma: M5308) for 15 h. Following 15 h, the media was removed and fresh media with AHA (0.1 mM) or MET (0.1 mM) were added. Muscle cells were then left unperturbed for 3-h, followed by collection of the conditioned media for analysis. Collected conditioned media was passed through a 0.22 μm strainer and concentrated (dialyzed) using Amicon 3 kDa filters (Millipore: UFC900308). The concentrated media was placed at −80°C for long-term storage. Protein concentration was determined using the Pierce BCA protein assay Kit (ThermoFisher Scientific: 23225).

Click-chemistry enrichment of muscle cell-derived azide-labeled proteins

The overarching principle of Bio-Orthogonal Non-Canonical Amino Acid Tagging (BONCAT) relies on the incorporation of amino acid analogs containing a functional group, specifically an azide, into the cellular proteome. Azidohomoalanine is a methionine analog which differs only in its unique azide moiety. The endogenous protein translation machinery recognizes AHA, and incorporates it into newly synthesized proteins in place of methionine.[30] Azide-bearing proteins—either cytosolic or those secreted into the conditioned media—can undergo affinity purification through introducing an alkyne-bound bead. The alkyne moiety forms a covalent bond with azide when in the presence of a copper catalyst, ultimately 'clicking' the azide and alkyne moieties together. As such, this approach only detects proteins synthesized within cells, circumventing the need for serum depletion. We and others have demonstrated the successful use of AHA in primary murine cell lines.[31,69] Our preliminary studies confirmed sufficient incorporation of AHA into the primary myofiber proteome, with 16 h showing greatest incorporation. All primary muscle cells from each participant successfully incorporated AHA into their respective proteome. Methionine-pulsed samples were used to determine specificity of protein enrichment. 3.5 mg of protein from each sample (20 mg for C2C12 samples) were used for click enrichment using the Click-iT Protein Enrichment Kit following the manufacturers protocol (Invitrogen: C10416). Following enrichment, protein-bound beads were placed at −80°C until follow-up proteomic analysis.

Proteomic processing of bead-bound proteins

Protein-bound beads, for both primary human skeletal muscle cells and C2C12 cells (described below), underwent reduction (10mM Dithiothreitol), alkylation (100 mM Iodoacetamide), and then on-bead digestion with Trypsin (Promega) for 3 h. Supernatant was extracted and proteins were then digested with Lys-C (FUJIFILM Wako) and Trypsin overnight. Digestion reactions were stopped with neat TFA. Samples then underwent Solid Phase Extraction and analyzed by LC-MS/MS using Thermo Scientific Orbitrap Fusion LUMOS coupled to a Thermo Scientific Easy-nLC 1200 system with a direct loading setup. Peptides were separated on a 100μm/12-cm pulled emitter C18 reversed-phase column (Nikkyo Technos; Catalog # NTCC-360/100-3-125) using a 70-min analytical gradient (BufferA:Buffer B composition being 1% acetonitrile,0.1% formic acid: 80% acetonitrile, 0.1% formic acid, with a %B gradient of 2–35% at 300 nL/min). The instrument was operated in high-resolution/high-mass-accuracy DDA (Data Dependent Acquisition) mode with optimized acquisition parameters. Raw data was processed through MaxQuant (v 2.6.6.0) software using either human or mouse databases to produce label-free quantification (LFQ) and intensity-based absolute quantification (iBAQ) values. LFQ and iBAQ values were then taken to Perseus to perform statistical analysis. Values were Log2 transformed and filtered to remove proteins that were either found by reverse search or as contaminants. iBAQ values were filtered to only include proteins that produced a value in 4 out of 6 replicates for at least one sample group for AHA vs. MET comparisons. For C2C12 cells, iBAQ values were filtered to only include proteins that produced a value in 2 out of 3 replicates for at least one sample group. "NaN" values

were then imputed with random low-abundant signals for statistical analysis purposes. Sample groups (MET vs. AHA) were plotted against each other in two-sample t-tests. For analysis of C2C12 cells following either the S-SIE or S-MIE contraction protocol, we first filtered for proteins which were significantly increased in expression within the conditioned media of AHA-treated samples (CTRL, MIE, and SIE) compared to the MET-treated control. iBAQ values were used for this initial filtering step. We then used LFQ values of all subsequent proteins to analyze differential expression between CTRL versus MIE or CTRL versus SIE.

Human iPSC-derived skeletal muscle cells and brown adipocytes

As an orthogonal strategy to identify muscle-fiber derived proteins, we characterized the secretome of human inducible pluripotent stem cell (iPSC)-derived skeletal muscle cells (iPSC-SKM). In addition, we generated iPSC-derived brown adipocytes (iPSC-BA) as a negative control. iPSC-BA were included because brown adipocytes originate from the same common progenitor as skeletal muscle cells,[70] yet take on distinct differentiation trajectories, permitting one to determine proteins preferentially released from skeletal muscle cells compared to a closely related non-muscle cell. iPSC-SKM were differentiated from NCRM1 (NIH CRM) human iPSC's as previously described and have been previously authenticated,[71,72] and is the same sample material used in Plucińska et al. 2025, where detailed cell differentiation and processing is described.[73] Following differentiation, conditioned media was collected from both iPSC-SKM and iPSC-BA and processed for Olink analysis as described previously. Olink NPX values were then analyzed using the Limma package in R.

C2C12 cell culturing

C2C12 mouse skeletal myoblasts were obtained from the American Type Culture Collection and grown in proliferative medium (PM) composed of DMEM (Thermo Fisher Scientific, Basel, Switzerland) supplemented with 10% fetal bovine serum (FBS) (Thermo Fisher Scientific, Basel, Switzerland), 100 IU/mL penicillin, 100 μg/mL streptomycin (Thermo Fisher Scientific, Basel, Switzerland) and 1% non-essential amino acids (Thermo Fisher Scientific, Basel, Switzerland), and maintained at 37°C in a humidified atmosphere with 5% CO_2. When myoblasts reached 80–90% confluence, differentiation was started by replacing the media with differentiation medium (DM; DMEM supplemented with 2% horse serum [Thermo Fisher Scientific, Basel, Switzerland]). On day 7 of differentiation, the DM was replaced with either DM-AHA or DM-MET. DM-AHA contained DMEM (21013–024, Thermo Fisher Scientific, USA), 2% of dialyzed horse serum, 100 IU/mL penicillin, 100 μg/mL streptomycin, 1% non-essential amino acids, 4 mM GlutaMax, 0.2 mM L-cystine, sodium pyruvate, and 0.1 mM AHA. For DM-MET, the media contained 0.1 mM L-Met instead of AHA.

Electrical stimulation of C2C12 myotubes

Differentiated myotubes (day 8 post differentiation) containing 4 mL of the respective DM (DM-AHA or DM-MET) were electrically stimulated (C-Pace EM stimulator, IONOPTIX LLC, MA, USA) as previously published.[32] In brief, to simulate moderate-intensity exercise (S-MIE) 1 h repeated stimulation at 14 V, 2 Hz and 2 ms pulse duration was used. To simulate sprint-interval exercise (S-SIE) 6 × 30 s pulse (5 s on, 1 s off) at 14 V, 50 Hz and 2 ms pulse duration with 4 min rest was used. The respective differentiation media (DM-AHA or DM-MET) was replaced 1 h before the electrical stimulation protocol. Following the exercise protocol, cells were allowed to rest in the incubator for another 3 h until samples were collected. The collected media was filter-sterilized (0.22 μm) and concentrated using Amicon 3 kDa filters (Millipore: UFC900308). The concentrated media was placed at −80°C for long-term storage. Protein concentration was determined using the Pierce BCA protein assay Kit (ThermoFisher Scientific: 23225).

Western blot analysis

Cell pellets from each well were resuspended in 100 μL of lysis buffer (20 mM Tris/HCl (pH 6.8), 2 mM EDTA (pH 8), 137 mM NaCl, 10% glycerol, 10% Triton X-100, 10 mM beta-glycerophosphate, 1 mM KH2PO4, 1 mM PMSF, 1 mM Na_3VO_4, 50 mM NaF, 10 mM NaPPi, containing a protease inhibitor mixture). The resulting lysate was gently sonicated and debris was removed by centrifugation at 9300 × g at 4°C for 10 min. Protein quantification was performed using the BCA Kit (Thermo Fisher Scientific, Ecublens, Switzerland). For each sample, 20 μg of protein were combined with 2× Laemmli sample buffer containing SDS and 2-mercaptoethanol (Bio-Rad, Hercules, CA, USA) and incubated for 3 min at 95°C. Samples were run on 4–15% SDS-precast gradient gels (Bio-Rad, Hercules, CA, USA) and transferred onto PVDF membranes. Total protein staining was detected on membranes with Total Protein Stain (Revert 700; LI-COR, Lincoln, NE, USA). Membranes were subsequently washed out and membranes were incubated for 1 h at room temperature with v/v PBS LI-COR blocking buffer (LI-COR, Lincoln, NE, USA). Then, membranes were incubated overnight at 4°C with primary antibody prepared in blocking buffer (Phospho-AMPK alpha (Thr172) #2535 and AMPK alpha #2793; Cell Signaling). Membranes were washed in PBS-T and incubated for 1 h at room temperature with secondary antibody IRDye 680-conjugated goat anti-mouse and IRDye 800-conjugated goat anti-rabbit IgG (1:10,000; LI-COR, Lincoln, NE, USA). Immunoreactive bands were visualized using infrared fluorescence (IR-Odyssey/Fc, LI-COR, Lincoln, NE, USA), and band densities were quantified using Image Studio v 6.1 (LI-COR, Lincoln, NE, USA).

Human skeletal muscle collection and RNA-sequencing

Participant information is described above (Cohort 1) and in Botella et al. 2024.[17] All data were sourced from this prior analysis, which included a sample size of $N = 14$ for each condition (MIE and SIE). In brief, skeletal muscle was collected under local anesthesia from

the *vastus lateralis* using the Bergström needle biopsy technique before and 3 h following exercise. Muscle tissue was blotted for residual blood and any remaining fat and connective tissue were carefully removed. The sample was then immediately frozen in liquid nitrogen and stored at −80°C. All RNA extraction, cDNA library, and RNA-sequencing can be found in Botella et al. 2024.[17]

RNA-sequencing

For all RNA-sequencing experiments, 100 ng of total RNA was used to generate RNA-Seq libraries using Illumina stranded mRNA kit (Catalog #: 20040534), following the manufactures protocol. Libraries prepared with unique dual indexes were pooled at equal molar ratios. The pool was sequenced on Illumina NextSeq 2000 P3 flowcell using NextSeq Control Software v1.7.1.46395 to generate 100 bp (or 50 bp) paired reads, following the manufactures protocol (Document #: 200027171 v04).

Data analysis for RNA-sequencing

Transcript abundance was determined from FASTQ files using Salmon (v1.8.0) and the Ensembl reference transcript sequences.[74] Transcript per million (TPM) values were calculated using the tximport R Bioconductor package (v1.22.0).[75] Differential gene expression analysis was performed with the DESeq2 R Bioconductor package (v 1.42.1).[76] For paired samples, differences in gene expression across time points or conditions were calculated while controlling for each subject in the linear model. Gene counts were transformed with the vst function from DESeq2 to apply a variance stabilizing transformation, and z-scores of these normalized values for the indicated gene sets were visualized with heatmaps generated using the pheatmap R package (v1.0.12).[68] For GSEA, the Wald statistic from the DESeq2 analysis was used to generate the ranked list of genes. The clusterProfiler R Bioconductor package (v4.12.6) was then used to perform GSEA to determine the enrichment of the Gene Ontology Biological Processes gene sets sourced using the msigdbr R package (v25.1.1).[77–79]

Identification of organ-enriched plasma proteins

To identify proteins in the plasma that were enriched in a particular tissue, bulk RNA raw read counts were downloaded from the GTEx portal (version 8) and normalized using the DESeq2 R Bioconductor package (v 1.44.0)[76]. The mean normalized count for each gene within a tissue was calculated, and a gene was determined to be enriched in a particular organ if the maximum expression value for the group of tissues belonging to that organ was four times the value of the maximum of the tissues for next highest organ. Organ identifiers, and their corresponding tissues, were sourced from Oh et al. 2023.[25] In brief, the different sub-tissues within GTEx were collapsed into their respective organ. For example, the adipose organ, which is comprised of distinct depots (e.g., subcutaneous and visceral adipose tissue), was collapsed into a single "Adipose" organ.

Prediction of organ-to-organ crosstalk

To predict organ-to-organ crosstalk, we leveraged a human receptor database sourced from CellTalkDB which includes all known or predicted ligand-receptor pairs upon a given cell-type.[34] To filter down the number of receptors, and determine those that are enriched within a given organ, we removed all known or predicted receptors which are not organ-enriched as determined by their GTEx gene expression levels described above. From the remaining list of receptors (Table S4), we overlaid the differentially regulated organ-enriched plasma proteins to identify ligands which have a known or predicted receptor from the remaining organ-enriched receptor dataset.

Primary human adipocyte media swap with exercised plasma

Abdominal subcutaneous adipose tissue was collected from healthy participants and the stromal vascular fraction (SVF) containing preadipocytes were isolated and purchased from Lonza (Catalog #: PT-5001; Lot #: 24TL271510; 25TL121766). Preadipocytes were subsequently plated and differentiated into mature adipocytes in 6-well collagen coated plates following the manufacturer's instructions. Due to the relatively short period in culture, cells were not tested for mycoplasma. Fully differentiated adipocytes were histologically multilocular and positive for adipocyte markers *FABP4*, *FASN*, and *PPARG*, compared to non-differentiated preadipocytes. Upon complete differentiation, adipocytes were washed twice with warm PBS, followed by a 30-min incubation with 900 μL of Lonza growth media (Catalog #: PT-8002) containing L-glutamine, recombinant human insulin, and gentamicin sulfate-amphotericin, without fetal bovine serum. Following 30 min, 100 μL of human plasma was added to each well. Plasma samples were from individuals undergoing either moderate-intensity exercise or sprint-interval exercise as described in Cohort 1. The resting (pre) or immediately post (0 h) plasma samples were used. Each time point from each individual were conducted in duplicate. Six participants for either SIE or MIE were used. One plasma sample from SIE resulted in adipocytes becoming detached, and was thus not used for downstream processing for the 12 h incubation experiment, and one adipocyte sample from the MIE group had poor RNA quality (RIN score <5) and was not used for downstream processing for the 3 h incubation experiment. Adipocyte cultures containing plasma were incubated at 37°C in a humidified incubator with 5% CO_2. Following 3 or 12 h, adipocytes were washed with ice-cold PBS and were immediately processed for RNA extraction. In brief, adipocytes were homogenized in Trizol (ThermoFisher Scientific: 15596026), and the RNA was separated via the Trizol-chloroform method. The subsequent RNA fraction was combined with 70% ethanol, which was then processed with the Qiagen RNeasy Plus Micro Kit (Qiagen: 74034), including DNAse treatment. High-quality RNA was processed for RNA-sequencing as described above.

UK BioBank association analysis

Plasma protein-disease associations for prevalent and incident diseases were retrieved from the Proteome-Phenome Atlas[44] (proteome-phenome-atlas.com). This cohort included 53,026 UK Biobank participants with plasma proteomic profiling performed using the Olink Explore platform, which is the same platform used in the present study. Plasma proteins from each of the 53,026 participants were assessed for their association with, or protection from, 1,066 incident or prevalent diseases. Within the UKBB dataset, diseases are grouped into 15 chapters that broadly reflect distinct body systems. Each chapter contains multiple disease categories, and a given protein can be associated with increased or decreased risk across multiple diseases. Protein-disease associations were considered statistically significant by having a Bonferroni-adjusted p-value of <0.05. Subsequent filtering for proteins of interest included identifying those that were 1) regulated by SIE or MIE, 2) protective from a given disease (i.e., HR/OR < 1), and 3) within a predefined disease category of interest (e.g., type 2 diabetes, metabolic disorders, or obesity). Datapoints for the heatmap in Figure 5B are displayed as Log_2HR whereas Figure 5C shows the Log_2FC. Gene ontology for biological processes were conducted with an adjusted-Fisher's Exact Test p-value of <0.05 considered statistically significant.

QUANTIFICATION AND STATISTICAL ANALYSIS

For all -omic-derived datasets described throughout the Results, including metabolomic, proteomic, and transcriptomic, their corresponding statistical analyses can be found in their respective sections of the STAR Methods. For the correlation analysis between the Olink-generated plasma proteome between each time point in the untrained and trained cohort (Figures S2D–S2G), a Pearson's product-moment correlation was used. Statistical significance was evaluated with two-tailed tests with significance set at $p < 0.05$. For the analysis of phosphorylated AMPK between EPS conditions, a one-way ANOVA with Tukey's post hoc test was used with significance set at $p < 0.05$. Throughout the Results, error bars indicate standard error of the mean.